Achievements and Challenges in Improving Air Quality in China: Analysis of the Long-Term Trends from 2014 to 2022

Zheng, Huang ; Kong, Shaofei ; Seo, Jihoon ; Yan, Yingying ; Cheng, Yi ; Yao, Liquan ; Wang, Yanxin ; Zhao, Tianliang ; Harrison, Roy

DOI:
10.1016/j.envint.2023.108361

Document Version
Publisher's PDF, also known as Version of record

Citation for published version (Harvard):
Zheng, H, Kong, S, Seo, J, Yan, Y, Cheng, Y, Yao, L, Wang, Y, Zhao, T & Harrison, R 2024, 'Achievements and Challenges in Improving Air Quality in China: Analysis of the Long-Term Trends from 2014 to 2022', *Environment international*, vol. 183, 108361. https://doi.org/10.1016/j.envint.2023.108361

Environment International 183 (2024) 108361

Contents lists available at ScienceDirect

Environment International

journal homepage: www.elsevier.com/locate/envint

Full length article

Achievements and challenges in improving air quality in China: Analysis of the long-term trends from 2014 to 2022

Huang Zheng [a,c], Shaofei Kong [a,b,c,*], Jihoon Seo [d], Yingying Yan [a,c], Yi Cheng [a], Liquan Yao [a], Yanxin Wang [a,c], Tianliang Zhao [b], Roy M. Harrison [e,f,*]

[a] Department of Atmospheric Sciences, School of Environmental Studies, China University of Geosciences, Wuhan 430078, China
[b] Collaborative Innovation Center on Forecast and Evaluation of Meteorological Disasters, Key Laboratory for Aerosol-Cloud-Precipitation of the China Meteorological Administration, PREMIC, Nanjing University of Information Science &Technology, Nanjing, China
[c] Research Centre for Complex Air Pollution of Hubei Province, Wuhan 430078, China
[d] Climate and Environmental Research Institute, Korea Institute of Science and Technology, Seoul 02792, Republic of Korea
[e] School of Geography, Earth and Environment Sciences, University of Birmingham, Birmingham B15 2TT, UK
[f] Department of Environmental Sciences, Faculty of Meteorology, Environment and Arid Land Agriculture, King Abdulaziz University, PO Box 80203, Jeddah, Saudi Arabia

ARTICLE INFO

Handling Editor: Xavier Querol

Keywords:
Air pollution
$PM_{2.5}$ reduction
O_3 pollution
Kolmogorov-Zurbenko filter
Emission and meteorology impact

ABSTRACT

Due to the implementation of air pollution control measures in China, air quality has significantly improved, although there are still additional issues to be addressed. This study used the long-term trends of air pollutants to discuss the achievements and challenges in further improving air quality in China. The Kolmogorov-Zurbenko (KZ) filter and multiple-linear regression (MLR) were used to quantify the meteorology-related and emission-related trends of air pollutants from 2014 to 2022 in China. The KZ filter analysis showed that $PM_{2.5}$ decreased by 7.36 ± 2.92% yr^{-1}, while daily maximum 8-h ozone (MDA8 O_3) showed an increasing trend with 3.71 ± 2.89% yr^{-1} in China. The decrease in $PM_{2.5}$ and increase in MDA8 O_3 were primarily attributed to changes in emission, with the relative contribution of 85.8% and 86.0%, respectively. Meteorology variations, including increased ambient temperature, boundary layer height, and reduced relative humidity, also contributed to the reduction of $PM_{2.5}$ and the enhancement of MDA8 O_3. The emission-related trends of $PM_{2.5}$ and MDA8 O_3 exhibited continuous decrease and increase, respectively, from 2014 to 2022, while the variation rates slowed during 2018–2020 compared to that during 2014–2017, highlighting the challenges in further improving air quality, particularly in simultaneously reducing $PM_{2.5}$ and O_3. This study recommends reducing NH_3 emissions from the agriculture sector in rural areas and transport emissions in urban areas to further decrease $PM_{2.5}$ levels. Addressing O_3 pollution requires the reduction of O_3 precursor gases based on site-specific atmospheric chemistry considerations.

1. Introduction

Over the past three decades, the rapid and energy-intensive economic growth in China has resulted in severe air pollution. Deterioration in air quality causes visibility impairment (Ding et al., 2016; Wang et al., 2018; Ma et al., 2020), adverse human health effects (Kan et al., 2012; Shiraiwa et al., 2017; Xiao et al., 2022), and changes in climate forcing (Fiore et al., 2012; von Schneidemesser et al., 2015; Gao et al., 2018). In early 2013, extensive regions in eastern and central China experienced a severe and long-lasting haze event, impacting a population of 800 million over an area of 1.3 million square kilometers (Huang et al., 2014). This event prompted an acceleration of China's air pollution control efforts.

To solve air pollution and protect the public from its potential health issues, China initiated the Air Pollution Prevention and Control Action (APPCA) in 2013 (Huang et al., 2018; Zheng et al., 2018; Zhang et al., 2019). As a result of its implementation, anthropogenic emissions of carbon monoxide (CO), nitrogen oxides (NO_x), inhalable particulate matter (PM_{10}), fine particulate matter ($PM_{2.5}$), and sulfur dioxide (SO_2) decreased by 23%, 21%, 36%, 33%, and 59%, respectively, in 2017

* Corresponding authors at: Department of Atmospheric Sciences, School of Environmental Studies, China University of Geosciences, Wuhan 430078, China (Shaofei Kong). School of Geography, Earth and Environment Sciences, University of Birmingham, Birmingham B15 2TT, UK (Roy M. Harrison).
E-mail addresses: kongshaofei@cug.edu.cn (S. Kong), r.m.harrison@bham.ac.uk (R.M. Harrison).

https://doi.org/10.1016/j.envint.2023.108361
Received 3 July 2023; Received in revised form 2 November 2023; Accepted 29 November 2023
Available online 30 November 2023

compared to those in 2013 (Zheng et al., 2018). The ambient $PM_{2.5}$ concentrations in China decreased (Song et al., 2017; Silver et al., 2018; Cheng et al., 2019; Xue et al., 2019), and a 32% decrease in the national population-weighted concentrations from 2013 to 2017 was reported (Xue et al., 2019). Despite the progress made through the APPCA, air quality in most cities (71%) still exceeded Chinese air quality standards (annual mean concentrations of 60 μg m^{-3} for SO_2, 40 μg m^{-3} for NO_2, 35 μg m^{-3} for $PM_{2.5}$ and 70 μg m^{-3} for PM_{10}, respectively, and daily mean value of 4 mg m^{-3} for CO and 160 μg m^{-3} for daily maximum 8-h ozone) in 2017 (https://www.gov.cn/guoqing/2019–04/09/content_5380689.htm). Subsequently, the Three-Year Action Plan (TYAP) was launched in 2018. The CO, NO_x, PM_{10}, $PM_{2.5}$, and SO_2 emissions decreased by 11.1 tera grams (Tg), 1.6 Tg, 1.0 Tg, 0.6 Tg, and 1.6 Tg, respectively in 2020 compared to those in 2018 (Geng et al., 2023). As a result, air quality during 2018–2020 was further improved and the non-attainment rate of air quality among 337 cities decreased to 40.1% in 2020 (https://www.cnemc.cn/jcbg/zghjzkgb/202105/t20210527_835035.shtml). The variations of air pollutants, however, are masked by meteorological variations. It can be difficult to judge whether a variation in air pollutant concentration is dominated by changes in meteorological conditions or emission strength (Grange and Carslaw, 2019). Without consideration of the effects of meteorology upon air pollutant concentrations can lead to erroneous assessments of the effectiveness of air pollution control measures in improving air quality (Vu et al., 2019; Shi et al., 2021).

To ensure a precise assessment of air quality improvement, it is essential to distinguish the influence of anthropogenic factors from meteorological factors on the variations of air pollutants (Seo et al., 2018; Chen et al., 2019; Zhai et al., 2019; Zhang et al., 2019; Zheng et al., 2020a, 2020b; Shi et al., 2021; Dai et al., 2022). Generally, two approaches are employed to accomplish it. The first approach involves utilizing a chemical transport model (CTM) that incorporates the emission inventory of air pollutants, together with atmospheric dynamical, physical, and chemical processes. The Weather Research and Forecasting Model-Community Multiscale Air Quality Model (WRF-CMAQ) (Cheng et al., 2019; Xue et al., 2019; Zhang et al., 2019) and the GEOS-Chem (Zhang et al., 2018a; Li et al., 2019a; Sun et al., 2019; Dang et al., 2021; Zhai et al., 2021; Qiu et al., 2022) are extensively utilized for this purpose. With the WRF-CMAQ modeling, Zhang et al. (2019) found that the changes in meteorological conditions only accounted for 9% of the total $PM_{2.5}$ reduction in China between 2013 and 2017. Li et al., (2019a) found that anthropogenic activities rather than meteorological conditions dominated ozone (O_3) increasing during 2013–2017 with the GEOS-Chem model. The uncertainties of this approach are mainly associated with emission biases (Yan et al., 2014, 2016) and incomplete physical–chemical mechanisms in the simulation schemes (Yan et al., 2019). Due to inadequate representation of secondary aerosol formation processes, chemical transport models face challenges in accurately reproducing the mass concentrations of organic aerosols and capturing their variability, particularly during haze episodes in China (Chen et al., 2017; Hallquist et al., 2016). Moreover, the time-consuming nature of updating emission inventories required in numerical models results in a gap between the study period and the year of available emission data, further limiting the applicability of CTM.

Statistical modeling, such as multiple-linear-regression (Li et al., 2019b, 2020; Zhai et al., 2019), Kolmogorov-Zurbenko (KZ) filter (Seo et al., 2018; Zheng et al., 2020b; Sun et al., 2022), and Random Forest models (Grange et al., 2018; Vu et al., 2019; Ji et al., 2023) is an alternative approach to study the contributions of emissions and meteorology to long-term changes in air pollutants. Unlike the CTM, these statistical models do not need an emission inventory as input; instead, they rely on a simple time series of air pollutants and meteorological parameters. Remarkably, the conclusions obtained from statistical models are comparable to those from CTM (Chen et al., 2019; Fang et al., 2022; Sun et al., 2022). For instance, it was estimated that emission reduction accounted for 78.6% of the $PM_{2.5}$ reduction in 2013–2017 in Beijing by the KZ filter. This finding was comparable to the results obtained from WRF-CMAQ modeling, which indicated a contribution of 80.6% from emission reduction (Chen et al., 2019). Considering the high computational costs and aforementioned uncertainties with CTM, statistical modeling can serve as an alternative and effective method to study the influence of meteorological conditions and anthropogenic emissions on the long-term variations of air pollutants, particularly in regions lacking reliable emission inventory.

Using the CTM and statistical methods, previous studies concerning the long-term trends of air pollutants and their drivers mainly focused on a certain period of clean air action, e.g., APPCA (Geng et al., 2019; Li et al., 2019b; Ma et al., 2019a; Vu et al., 2019; Zhang et al., 2019; Maji et al., 2020; Zhao et al., 2021) or TYAP (Dai et al., 2022; Du et al., 2022; Liu et al., 2023a) in China. The policy-driven changes in air pollutant emission varied between APPCA and TYAP (Geng et al., 2023), which has impacts on air pollutant long-term trends. The comprehensive study concerning the drivers of air pollutant variations in different phases of clean air actions and their comparison was less reported (Liu et al., 2023a). Additionally, the inter-annual changes in meteorology also contribute to the variations in air pollutants (Mao et al., 2016; Lin et al., 2022; Shen et al., 2023). Previous studies mainly focused on the overall impacts of meteorological conditions on air pollutant variations (Vu et al., 2019; Zhai et al., 2019; Zhang et al., 2019; Mousavinezhad et al., 2021), while the impacts of different meteorological factors were less investigated (Chen et al., 2020a, 2020b).

Therefore, this study aimed to (1) calculate the emission-related and meteorology-related long-term trends of $PM_{2.5}$ and O_3 from 2014 to 2022 using the KZ filter and multiple-linear regression, (2) compare the emission-related trends of $PM_{2.5}$ and O_3 during APPCA (2014–2017) and TYAP (2018–2020), (3) identify the dominant meteorological factor to the variations of $PM_{2.5}$ and O_3, and (4) discuss the achievements of present air pollution control measures and explore the possible countermeasures for further reducing $PM_{2.5}$ levels and alleviating O_3 pollution in China. This work can serve as a valuable reference to understand the relationship between air pollutant emissions and atmospheric concentrations on a global scale within the context of a changing climate.

2. Methodology

2.1. Data sources and preprocessing

Hourly concentrations of air pollutants, including CO, NO_2, O_3, PM_{10}, $PM_{2.5}$, and SO_2, were obtained from a widely used public database (https://beijingair.sinaapp.com/) (Silver et al., 2018; Fan et al., 2020; Zheng et al., 2023) for the period between 2014-05-13 and 2022-12-31. For the pre-2014-5-13 period, hourly observations of air pollutants were downloaded from https://data.epmap.org/page/index. It should be noted that the data reported by the two different platforms were from the national air quality monitoring network established and operated by the China National Environmental Monitoring Center. The overall data quality of this dataset has been considered reliable since 2013 (Liang et al., 2016). However, some data quality issues were identified, such as instances where $PM_{2.5}$ levels were higher than PM_{10} during certain periods, as well as the presence of outliers in time series. Furthermore, the conditions to calculate the air pollutant concentrations were revised from the standard condition (273 K and 101.325 kPa) to the reference condition (298 K and 101.325 kPa) since 2018-09-01. To address these concerns, data quality control and quality assurance procedures were performed. To remove the outliers, the hourly concentrations in each site were scaled into the dataset with mean value and standard deviation of 0 and 1 respectively. In line with previous studies (Song et al., 2017; Silver et al., 2018), the following rules were used to judge the outliers: (1) have an absolute z score of larger than 4 ($|z_t| > 4$); (2) have an increment from the previous value as larger than 9 ($z_t - z_{t-1} > 9$); (3) have a ratio of the value to its centered rolling mean of order 3 (RM3) larger than 2 ($z_t/\mathrm{RM3}\ (z_t) > 2$). After conducting data quality control

and assurance, the changes in mean hourly air pollutant concentrations were determined. The adjustments in mean (± standard deviation and hereafter) hourly concentrations, before and after data quality control, were found to be 0.15 ± 1.22, 0.01 ± 0.05, 0.02 ± 0.13, 0.12 ± 0.23, 0.05 ± 0.12, and 0.002 ± 0.07 μg m^{-3} for CO, NO_2, O_3, PM_{10}, $PM_{2.5}$, and SO_2, respectively (site-specific changes are provided in Table S1). To guarantee an adequate number of observations to calculate annual mean value, a threshold of 75% for each year's data availability was applied, resulting in a selection of 624, 615, 625, 496, 621, and 627 stations for CO, NO_2, O_3, PM_{10}, $PM_{2.5}$, and SO_2, respectively (see Table S2 in the supplementary materials for details). Finally, daily concentrations of CO, NO_2, PM_{10}, $PM_{2.5}$, and SO_2 were calculated based on sufficient hourly observations (> 18 h). Additionally, the daily maximum 8-h ozone (MDA8 O_3) was calculated as the maximum of 8-hour rolling average from 08:00 to 24:00 within a day.

Hourly values of surface meteorological parameters including temperature at 2 m (T2M, K), dewpoint at 2 m (D2M, K), mean sea level pressure (MSP, Pa), the eastward and northward component of wind at 10 m (U10, V10, m s^{-1}), total precipitation (TP, mm), boundary layer height (BLH, m), downward UV radiation at the surface (SSR, J m^{-1}), and total cloud cover (TCC, unitless) were derived from the ERA5 reanalysis (Hersbach et al., 2023). The U10 and V10 components of wind were used in this study for that they not only contained wind speed information but also had direction information to better understand the regional transport of air pollutants. The relative humidity (RH) was calculated using T2M and D2M (Dutton, 1976). Site-specific meteorological conditions were extracted using bi-linear interpolation. Anthropogenic air pollutant emissions from 2014 to 2020 were from the Multi-resolution Emission Inventory Model for China (MEIC) version 1.4 (https://meicmodel.org/cn/#firstPage) and more details about the latest version of MEIC can be found elsewhere (Geng et al., 2023).

2.2. Separating the emission-related and meteorology-related trends

The day-to-day time series of daily air pollutant concentration can be mainly divided into long-term, seasonal, and short-term components (Rao and Zurbenko, 1994). Each component is related to variations in emissions and meteorology. For instance, the long-term component is associated with the long-term changes in regional and local emissions resulting from socioeconomic policies and the long-term variations in meteorological conditions (Seo et al., 2018). To separate the three different components from the day-to-day variation of air pollutants, the KZ filter was used in this study. The KZ filter, here denoted as $KZ_{(m,p)}$ calculates the moving average of time with m (days) for p times iteration to remove the high-frequency components of a time series that are smaller than the effective filter width N ($\geq m \times p^{1/2}$) (Rao and Zurbenko, 1994; Rao et al., 1995, 1997). The moving average is defined as (Rao and Zurbenko, 1994):

$$Y_i = \frac{1}{m}\sum_{j=-k}^{k} X_{i+j} \quad (1)$$

where $i = 0, \pm 1, \pm 2, \ldots$, be a real-valued time series; $m = 2k + 1$ and k is the half-length of the simple moving average. The Y_i becomes the input for the second pass and so on. The KZ filter result is not sensitive to missing values and outliers due to the iterative moving average processes (Eskridge et al., 1997). In this study, $KZ_{(15, 5)}$ and $KZ_{(365, 3)}$ filters were used to filter out the short-term component (with a variability less than 33 days) and to leave the long-term component (with a variability longer than 1.7 years), respectively (Seo et al., 2018).

The original concentrations of air pollutants ($\chi(t)$) are usually log-normally distributed. It is necessary to transform the original concentrations into the log-transformed time series ($X(t) = \ln\chi(t)$) before the KZ filter analysis (Seo et al., 2018). The temporal signals of air pollutants (X (t)) at a given station can be separated into short-term ($X_{ST}(t)$), seasonal ($X_{SN}(t)$), and long-term ($X_{LT}(t)$) components (Seo et al., 2018):

$$X(t) = X_{ST}(t) + X_{SN}(t) + X_{LT}(t) = X_{ST}(t) + X_{BL}(t) \quad (2)$$

The sum of seasonal and long-term components is the baseline component ($X_{BL}(t) = X_{SN}(t) + X_{LT}(t)$), and it can be easily decomposed by applying the $KZ_{(15, 5)}$ filter to X(t), which filters out the white-noise-like $X_{ST}(t)$ as follow (Seo et al., 2018):

$$X_{BL}(t) = KZ_{(15, 5)}[X(t)] = X(t) - X_{ST}(t) \quad (3)$$

The $X_{BL}(t)$ is assumed to be the sum of its repeated climatological seasonal cycle (X_{BL}^{clm}) and residuals (ε) (Seo et al., 2018):

$$X_{BL}(t) = X_{BL}^{clm}(t) + \varepsilon(t) \quad (4)$$

where X_{BL}^{clm} (t) is the climatological seasonal cycle of the baseline and it is calculated as a composite mean of the baseline on each date repeating every year. Although X_{BL}^{clm} (t) accounts for most of the seasonality in X_{BL} (t), ε (t) still occupies small fractions of seasonal variability unconsidered in X_{BL}^{clm} (t) and the $X_{LT}(t)$. Applying the $KZ_{(365, 3)}$ filter to the residuals (ε), the long-term component (X_{LT}) and seasonal component (X_{SN}) can be obtained (Seo et al., 2018):

$$X_{LT}(t) = KZ_{(365, 3)}[\varepsilon(t)] = X_{BL}(t) - X_{SN}(t) \quad (5)$$

The long-term variability in air pollutants can be affected by both the changes in emissions and meteorological conditions. Therefore, $X_{LT}(t)$ is assumed to be the sum of the emission-related long-term component (X_{LT}^{EMI} (t)) and meteorology-related long-term component (X_{LT}^{MET} (t)), and the $X_{BL}(t)$ can be expressed as follows (Seo et al., 2018):

$$X_{BL}(t) = X_{SN}(t) + X_{LT}^{MET}(t) + X_{LT}^{EMI}(t) \quad (6)$$

The $X_{LT}(t)$ can be decomposed into the X_{LT}^{EMI} (t) and X_{LT}^{MET} (t) by the multiple-linear regression model (KZ-MLR) (Seo et al., 2018). In this study, the baseline components of meteorological variables (MET_{BL}) including T2M, MSL, U10, V10, RH, TP, BLH, SSR, and TCC were used. The multiple-linear-regression model between the baseline components of air pollutants ($X_{BL}(t)$) and meteorological parameters ($MET_{BL}(t)$) is expressed as (Seo et al., 2018):

$$X_{BL}(t) = a_0 + \sum_i a_i MET_{BL_i}(t) + \varepsilon'(t) \quad (7)$$

where ε' is the sum of the non-meteorological long-term variability (X_{LT}^{EMI} (t)) and the minor seasonal variability unexplained by the multiple-linear-regression model (ε'(t) – X_{LT}^{EMI} (t)). By removing the minor seasonality from ε'(t) using the $KZ_{(365, 3)}$ filter, X_{LT}^{EMI} (t) can be isolated as follows (Seo et al., 2018):

$$X_{LT}^{EMI}(t) = KZ_{(365,3)}[\varepsilon'(t)] = X_{LT}(t) - X_{LT}^{MET}(t) \quad (8)$$

Then X_{LT}^{MET} (t) can be simply obtained by subtracting X_{LT}^{EMI} (t) from $X_{LT}(t)$. The detailed decomposition procedure is described and schematically summarized with the $PM_{2.5}$ time series as an example (Fig. S1). The linear trends of the total, meteorology-related, and emission-related long-term components were calculated as the slope of the linear regression between time (year) and each component (i.e., $X_{LT}(t)$). The long-term linear trend of $X_{LT}(t)$ represents a fraction change rate (% yr^{-1}) of the baseline concentrations ($X_{BL}(t)$). The fraction change rate can be converted into an equivalent concentration change rate (μg m^{-3} yr^{-1}) by multiplying it with the temporal mean of the baseline component of the original time series (χ_{BL}) for the analysis period (Seo et al., 2018).

Site-specific and air pollutant-specific variance analysis of different components (Table S3) suggested that the meteorological influences on air pollutants were substantially explained and effectively removed by the KZ filter (see Text S1 for details). Similarly, the statistical metrics (Text S2) for different pollutants in each site (Table S4) suggested the high performance of KZ-MLR to decompose the long-term trends of air

pollutants into meteorology-related and emission-related trends (see Text S1 for details).

2.3. Identification of the dominant meteorological factor

To determine the primary meteorological factor influencing the long-term variations of air pollutants, an interpretable machine learning method was employed in this study. The Shapley Additive ExPlanation (SHAP) approach was utilized to quantify the contribution of each meteorological factor to the dependent observation. This method, based on game theory, calculates the importance of a predictor by measuring the difference in outputs when the predictor is included or excluded from the model. To establish the relationship between the meteorology-related long-term concentration of air pollutants (X_{LT}^{MET}) and the long-term components of meteorological variables (MET_{LT}), a linear regression model was constructed. The SHAP value, representing the local explanation, was computed for each meteorological factor for each observation. The aggregation of individual results provides an understanding of the overall impact of each meteorological variable on X_{LT}^{MET}, reported as a global explanation. The aggregated result for each meteorological factor was obtained by averaging the absolute values of the SHAP values (mean |SHAP|). By analyzing the aggregated SHAP values, the dominant meteorological factor affecting the long-term trend of air pollutants was identified as the variable with the highest value. Further information regarding the SHAP approach can be found in Text S3 and previous studies (Lundberg and Lee, 2017; Stirnberg et al., 2021; Zheng et al., 2023).

2.4. Regions of interest, data analysis, and visualization

In addition to the Beijing-Tianjin-Hebei (BTH: 37–41°N, 114–118°E), Yangtze River Delta (YRD: 30–33°N, 118–122°E), and Pearl River Delta (PRD: 21.5–24°N, 112–115.5°E), we also focused on the concentrations and trends of air pollutants in the other three key regions including Fenwei Plain (FWP: 33–35°N, 106.25–111.25°E, 35–37°N, 108.75–113.75°E.), Sichuan Basin (SCB: 28.5–31.5°N, 103.5–107°E), and Twain-Hu Basin (THB: 28.5–31.5°N, 110.75–114.75°E). The number of stations for $PM_{2.5}$ (MDA8 O_3) analysis was 48 (45), 41 (41), 54 (54), 39 (38), 21 (21), and 62 (62) in BTH, FWP, PRD, SCB, THB, and YRD, respectively.

Data analysis was conducted using R (R Core Team, 2023). The "kza" package (Close et al., 2018) was used for the KZ filter analysis. The model performance statistics were calculated using "openair" (Carslaw and Ropkins, 2012). The "fastshap" (Brandon, 2023) was used to calculate the SHAP value. All the figures in this study were generated by "ggplot2" (Hadley, 2016) and its extensions. Other packages (i.e., "reshape2", "lubridate", and "plyr") used in this study were available at the Comprehensive R Archive Network (CRAN, https://cran.r-project.org). All scripts to process and visualize data can be found at https://github.com/zh-cug/KZ-AP.

3. Results

3.1. Improved air quality during 2014–2022 in China

The annual mean values of air pollutants from 2014 to 2022 are summarized in Table S5, and the changes in their annual mean concentrations between 2014 and 2022 are shown in Fig. 1. A general

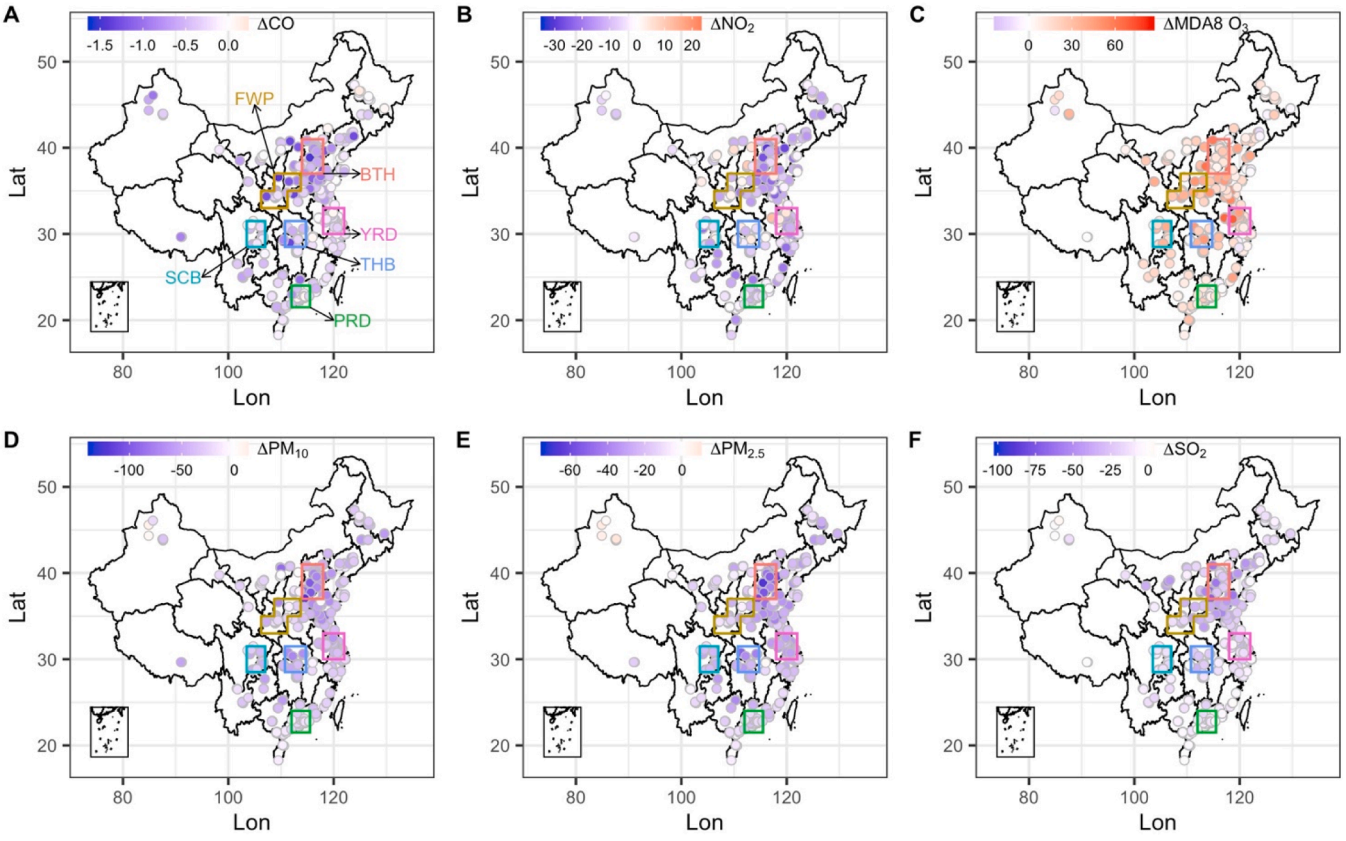

Fig. 1. Changes in annual mean mass concentrations of air pollutants (mg m^{-3} for CO and μg m^{-3} for other pollutants) between 2014 and 2022 in China (Δ = concentration in 2022 – concentration in 2014). The colored polygons represent the six key air pollution control regions including Beijing-Tianjin-Hebei (BTH), Fenwei Plain (FWP), Pearl River Delta (PRD), Sichuan Basin (SCB), Twain-Hu Basin (THB), and Yangtze River Delta (YRD) as shown in panel a. The detailed number of stations for air pollutants is provided in Table S2.

decrease in the mass concentrations of air pollutants was observed over China during this period. SO_2 showed the highest decrease of 63.6 ± 21.8%, followed by $PM_{2.5}$ (42.3 ± 13.9%), PM_{10} (40.1 ± 13.5%), CO (33.6 ± 19.7%), and NO_2 (23.6 ± 23.4%). MDA8 O_3 concentrations in China, however, increased by 37.3 ± 48.6%, rising from 77.4 ± 17.8 μg m^{-3} in 2014 to 99.6 ± 11.2 μg m^{-3} in 2022. The large standard deviation in national averages of air pollutants suggested the high spatial heterogeneity. Among the six key regions studied, the BTH region had the highest decreases in CO (51.9 ± 10.3%), NO_2 (36.9 ± 12.7%), PM_{10} (53.6 ± 6.23%), $PM_{2.5}$ (54.4 ± 9.01%), and SO_2 (82.7 ± 6.42%), while the THB region had the highest increase in MDA8 O_3 (73.4 ± 71.4%) (Table S6).

According to the new air quality guidelines set by the World Health Organization (WHO) in Sep 2021 (World Health Organization, 2021), the national annual concentrations of $PM_{2.5}$ (30.8 μg m^{-3}), PM_{10} (57.4 μg m^{-3}), and NO_2 (25.2 μg m^{-3}) in 2022 have achieved interim target I (< 35 μg m^{-3} for $PM_{2.5}$ and < 70 μg m^{-3} for PM_{10}) and interim target II (< 30 μg m^{-3} for NO_2), respectively. The further air quality improvement issue in China is primarily the complex pollution by $PM_{2.5}$ and O_3. Therefore, we mainly focused on $PM_{2.5}$ and O_3 in the following sections (other air pollutants were also calculated and results are provided in the supplementary tables, e.g., Table S7).

3.2. Long-term trends of $PM_{2.5}$ and MDA8 O_3 from 2014 to 2022

The time series of long-term trends (X_{LT}), emission-related (X_{LT}^{EMI}), and meteorology-related (X_{LT}^{MET}) trends of $PM_{2.5}$ and MDA8 O_3 are shown in Fig. 2. The spatial distribution of long-term, emission-related, and meteorology-related trends of $PM_{2.5}$ and MDA8 O_3 are shown in Fig. 3 and Fig. 4, respectively. Overall, most monitoring stations showed decreasing trends of $PM_{2.5}^{LT}$, with a national average of −7.36 ± 2.92% yr^{-1}. Among the six key regions (Table S8), the BTH region showed the highest decreasing rate of $PM_{2.5}^{LT}$ (−10.3 ± 3.44% yr^{-1}), followed by YRD (−9.28 ± 1.52% yr^{-1}), THB (−8.01 ± 2.30% yr^{-1}), PRD (−7.36 ± 1.33% yr^{-1}), SCB (−6.52 ± 1.73% yr^{-1}), and FWP (−5.00 ± 1.91% yr^{-1}). Among the long-term trends of $PM_{2.5}^{LT}$, the emission-related trends dominated with a national mean value of −6.09 ± 2.60% yr^{-1}. In line with the spatial distributions of $PM_{2.5}^{LT}$, the highest variation rate of $PM_{2.5}^{EMI}$ was found in BTH (−8.88 ± 3.14% yr^{-1}), while the lowest rate was observed in FWP (−3.86 ± 1.67% yr^{-1}) (Fig. 3e). The variations in meteorological conditions were also contributed to the reduction of $PM_{2.5}$ with a national mean value of −1.27 ± 0.82% yr^{-1} for $PM_{2.5}^{MET}$. Contrary to the spatial distributions of $PM_{2.5}^{LT}$ and $PM_{2.5}^{EMI}$, the highest reduction rate of $PM_{2.5}^{MET}$ was found in THB (−2.45 ± 0.45% yr^{-1}), followed by BTH (−1.44 ± 0.36% yr^{-1}), YRD (−1.44 ± 0.46% yr^{-1}), FWP (−1.14 ± 0.39% yr^{-1}), SCB (−1.07 ± 0.39% yr^{-1}), and PRD (−0.12 ± 0.29% yr^{-1}) (Fig. 3f).

In contrast, MDA8 O_3^{LT} showed an increasing trend with an average of 3.71 ± 2.89% yr^{-1} in China with the highest increasing trend of MDA8 O_3^{LT} in THB (5.29 ± 2.68% yr^{-1}), followed by FWP (5.13 ± 1.87% yr^{-1}), SCB (3.98 ± 2.70% yr^{-1}), PRD (3.74 ± 2.06% yr^{-1}), BTH (3.74 ± 2.36% yr^{-1}), and YRD (3.37 ± 3.03% yr^{-1}). The increasing trend of MDA8 O_3^{LT} was dominated by the emission-related trend with a national mean value of 3.40 ± 2.59% yr^{-1}. The variations in emissions contributed to the increase of MDA8 O_3^{LT} in six regions with the highest increasing rate in FWP (5.50 ± 1.68% yr^{-1}), followed by BTH (4.35 ± 2.17% yr^{-1}), THB (4.21 ± 2.18% yr^{-1}), SCB (3.87 ± 2.24% yr^{-1}), YRD (2.69 ± 2.58% yr^{-1}) and PRD (2.47 ± 1.77% yr^{-1}) (Fig. 4e). For the meteorology-related trend of MDA8 O_3, it was estimated to be 0.32 ± 0.83% yr^{-1}, suggesting that meteorological variations from 2014 to 2022 contributed to the enhancement of O_3 in China. On the regional scale, the meteorological conditions contributed to the increase of O_3 in most regions in China, except for BTH and FWP, where the meteorology-related trends were estimated as −0.61 ± 0.41% yr^{-1} and −0.36 ± 0.47% yr^{-1}, respectively (Fig. 4f). The regional differences in meteorology-related trends were detailly discussed in section 4.2.

Using the linear regressions between emission-related, meteorology-related trends, and long-term trends of air pollutants, the relative contributions of emissions and meteorology to air pollutant changes were quantified (Fig. S2). On a national scale, emission variations accounted for 85.8% of the reduction in $PM_{2.5}$. Similarly, the enhancement of

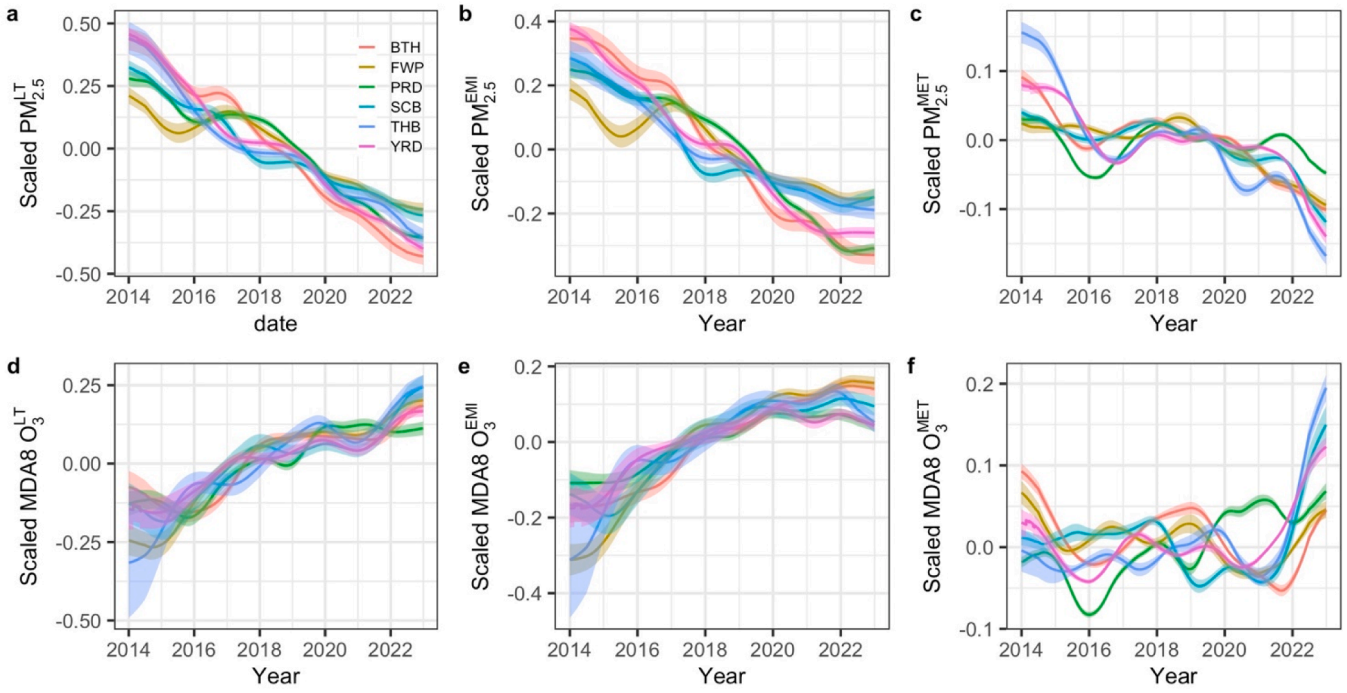

Fig. 2. Time series of scaled concentrations (unitless) of long-term (LT), emission-related (EMI), and meteorology-related (MET) for $PM_{2.5}$ (a–c) and MDA8 O_3 (d–f) from 2014 to 2022 in different regions. The concentrations of air pollutants during the study period were log-transformed in each station before KZ filter analysis. The regional mean values (solid lines) and their 95% confidence interval values (filled ribbons) were then calculated.

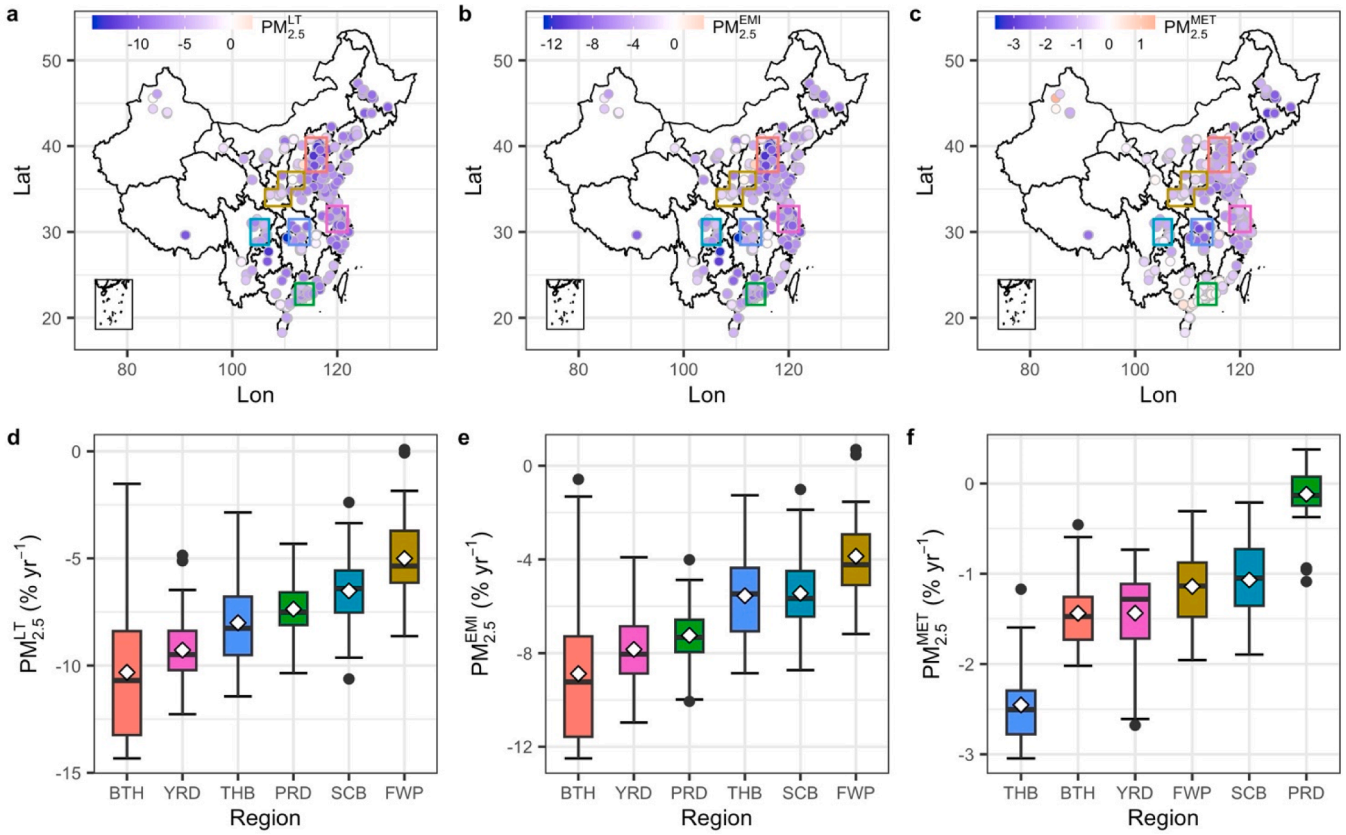

Fig. 3. Spatial distributions (a–c) and boxplots (d–f) of long-term ($PM_{2.5}^{LT}$, a, d), emission-related ($PM_{2.5}^{EMI}$, b, e) and meteorology-related ($PM_{2.5}^{MET}$, c, f) trends (% yr^{-1}) of $PM_{2.5}$ in China from 2014 to 2022.

MDA8 O_3 from 2014 to 2022 was primarily attributed to emissions, contributing to 86.0% of the increase. Regionally, emission variations also dominated the reduction of $PM_{2.5}$, with the highest contribution found in YRD (97%). Unlike the positive impact of emission variations on $PM_{2.5}$ reduction, they had a dominant effect on the increase in MDA8 O_3 concentrations in China, with the highest contribution in BTH (91%) and the lowest contribution in SCB (81%). The results here suggested the efforts in emission reduction were the primary driving force behind variations of $PM_{2.5}$ and O_3 in China, which was in line with the previous studies (Wang et al., 2019; Liu et al., 2023a; Zheng et al., 2023).

3.3. Comparison with previous studies

The decreasing trend in $PM_{2.5}$ and the increasing trend in O_3 have been widely reported since the application of APPCA in China (Table S9). For instance, Zhai et al. (2019) estimated a reduction rate of -5.2 μg m^{-3} yr^{-1} for $PM_{2.5}$ over the 2013–2018 period with the highest reduction rate in BTH (-9.3 μg m^{-3} yr^{-1}). Similarly, 97% of Chinese urban areas showed a decrease of $PM_{2.5}$ with an average of -3.5% yr^{-1} between 2010 and 2019 (Sicard et al., 2023a). On the contrary, the summer MDA8 O_3 showed an increasing trend of 1.9 ppb yr^{-1} (Li et al., 2020) or 5% yr^{-1}(Yin et al., 2021) in China from 2013 to 2019. Similarly, Mousavinezhad et al. (2021) reported an increasing trend of 3.3 μg m^{-3} yr^{-1} for MDA8 O_3 across China from 2015 to 2019 by KZ filter. To facilitate a more meaningful comparison with previous studies using the KZ-MLR method, we constrained our study's period to align with the durations reported in previous research. As shown in Fig. 5a, the long-term $PM_{2.5}$ trends from previous studies were generally lower than those in this study. For instance, Gao et al. (2022) estimated a regional average of -6.23 ± 2.47 μg m^{-3} yr^{-1} for $PM_{2.5}$ in 13 cities within BTH during 2018–2020 using the KZ filter coupled with stepwise MLR. This regional average was smaller than that in this study (-4.72 ± 2.04 μg m^{-3} yr^{-1}). Comparable results for $PM_{2.5}^{LT}$ during 2015–2021 were found in Wuxi, Hefei, and Jinhua between the research of Zhu et al. (2023) and this study. Similarly, this study and previous studies found increasing trends in MDA8 O_3 for various regions. For instance, MDA8 O_3^{LT} showed increasing trends of 4.2 μg m^{-3} yr^{-1} during 2014–2018 (Chen et al., 2020b) and 3.36 μg m^{-3} yr^{-1} during 2015–2019 (Mousavinezhad et al., 2021) in BTH. An exception to this was MDA8 O_3^{LT} in SCB, which showed a slight decrease during 2015–2019 (Mousavinezhad et al., 2021) while it showed an increasing trend in this study (Fig. 5b). These differences may arise from input variables for the model building, the methodology employed (e.g., stepwise MLR vs MLR), and the number of stations, etc. Despite the differences in rates of increase/decrease and the contributions of emission/meteorology between this study and previous studies, it is undeniable that emission variations dominate the reduction of $PM_{2.5}$ and the increase in O_3 in China (Fig. 5).

4. Discussion

4.1. Slowed variation rates of $PM_{2.5}$ and MDA8 O_3 from APPCA to TYAP

Due to the different measures between APPCA and TYAP (see Text S4 for details), the change rates of air pollutants varied between the two periods. As shown in Fig. S3, it was evident that the increase in O_3 during TYAP was lower than that during APPCA in all six regions. For instance, in BTH, MDA8 O_3 increased by 17.9% from 2014 to 2017, while it only increased by 1.1% from 2018 to 2020. On the contrary, the decrease in $PM_{2.5}$ during TYAP was lower than that during 2014–2017 in the BTH, SCB, THB, and YRD. To better understand the impact of emission variation on the slowed changes of O_3 and $PM_{2.5}$, the KZ-MLR was used to calculate the emission-related trends of air pollutants during APPCA and TYAP. It should be noted that the KZ filter can filter out trends longer

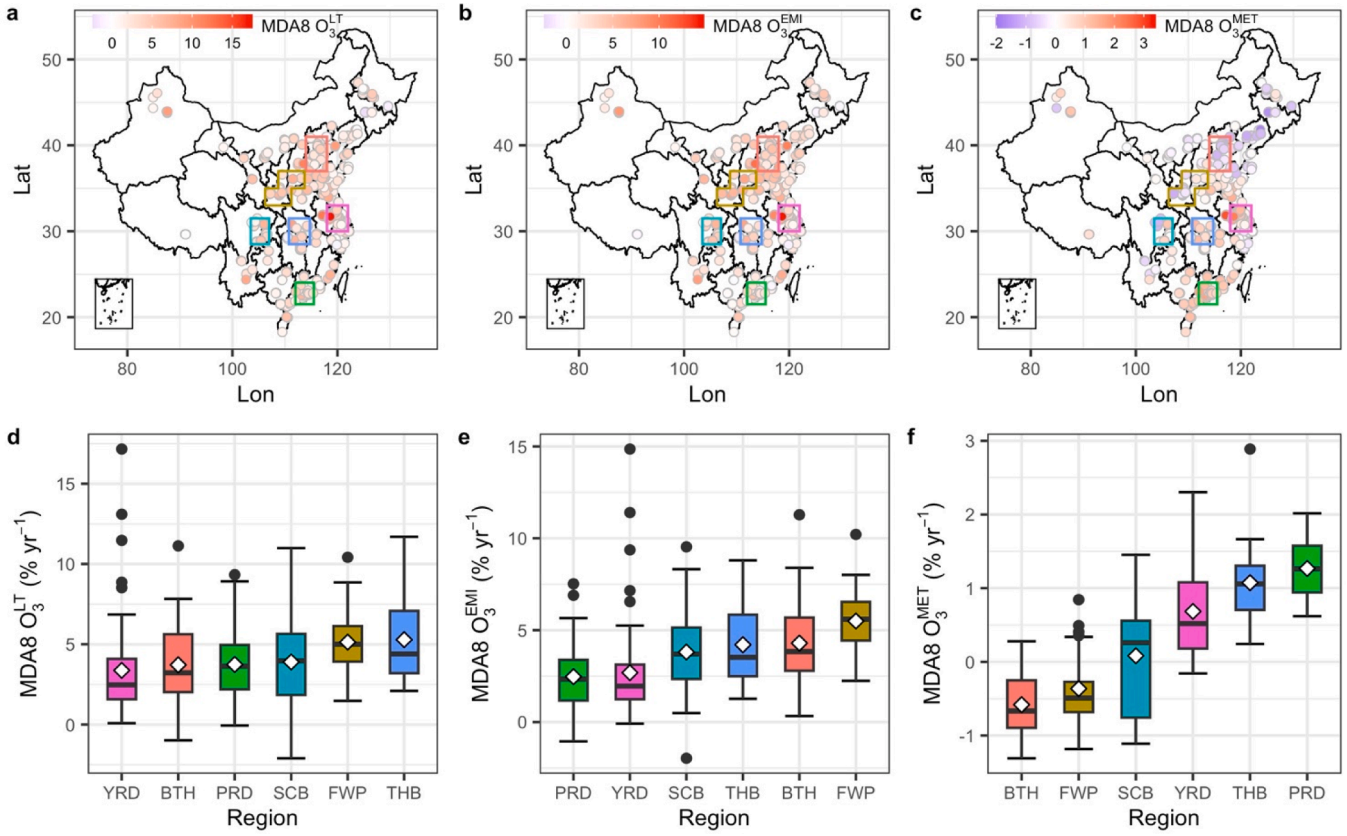

Fig. 4. Spatial distributions (a–c) and boxplots (d–f) of long-term (MDA8 O_3^{LT}, a, d), emission-related (MDA8 O_3^{EMI}, b, e) and meteorology-related (MDA8 O_3^{MET}, c, f) trends (% yr^{-1}) of MDA8 O_3 in China from 2014 to 2020.

than 1.7 years. Therefore, 4-year and 3-year observations for APPCA and TYAP were sufficient to get the long-term trends in this study. It also should be noted that our study period covered the year 2020, the emission of which was impacted by COVID-19. The emission reductions due to COVID-19 lockdowns were estimated as 1.84 Tg, 0.11 Tg, 0.09 Tg, and 0.31 Tg for CO, primary $PM_{2.5}$, SO_2, and VOC, respectively (Zheng et al., 2021). These reductions due to COVID-19 contributed 16.7%, 16.7%, 5.69%, and 14.5%, respectively to the total reductions of CO, primary $PM_{2.5}$, SO_2, and VOC between 2020 and 2018, suggesting the dominant role of clean air actions in emission reduction during TYAP. Although air pollutant concentrations showed significant reductions during COVID-19 (Sokhi et al., 2021), emissions of these pollutants rebounded in April as the spread of COVID-19 controlled, ultimately returning to levels comparable to those in 2019 (Zheng et al., 2021). Consequently, air pollutant concentrations also rebounded to levels similar to those observed in 2019 by the end of 2020 (Dai et al., 2022). Therefore, COVID-19 had limited impacts on the variation rates of air pollutants during TYAP (Dai et al., 2022).

As shown in Fig. 6a, the lower reduction rates for SO_2 during TYAP were found in six regions. On the contrary, NO_2^{EMI} showed a higher reduction during TYAP compared to that during APPCA (Fig. 6b), which was in line with a previous study (Geng et al., 2023). For $PM_{2.5}^{EMI}$ and PM_{10}^{EMI}, the lower reduction rates of $PM_{2.5}$ and PM_{10} were found in BTH, SCB, THB, and YRD during TYAP. For instance, in BTH, the reduction rate for $PM_{2.5}^{EMI}$ was -2.78 ± 1.82 μg m^{-3} yr^{-1} during 2018–2020, which was lower than that during 2014–2017 (-5.40 ± 3.26 μg m^{-3} yr^{-1}). Contrary to these four regions, FWP and PRD had higher reduction rates of $PM_{2.5}^{EMI}$ and PM_{10}^{EMI} during TYAP compared to those during APPCA (Fig. 6d, e), which can be attributed to the rebound in PM concentrations in these two regions during APPCA. Specifically, the $PM_{2.5}$ concentrations in 2016 and 2017 were higher than those in 2015 during APPCA, while it continuously declined from 2018 to 2020 in FWP and PRD (Fig. S3).

As shown in Fig. S4, the majority of air pollutants showed higher emission reductions during APPCA compared to those during TYAP. This was due to the implementation of extensive end-of-pipe measures (e.g., the majority of ultra-low emission technologies were implemented before 2017) during APPCA, while the efficacy of these measures noticeably declined after 2017, leading to a deceleration in emission reductions during TYAP (Geng et al., 2023). An exception to this was VOC emissions. Due to the overlook of VOC emissions, the VOC emissions increased by 1.2 Tg during APPCA, while it reduced by 2.2 Tg during TYAP due to the targeted measures such as the shutdown of small factories, the implementation of highly efficient collection facilities, and the promotion of water-based paints (Geng et al., 2023). As a result of both reductions from NO_x and VOC during TYAP, the increasing rates of MDA8 O_3^{EMI} during TYAP were lower than those during APPCA in six key regions (Fig. 6c). These results suggested that emission reduction measures targeting O_3 precursors may have a positive effect on mitigating O_3 levels between 2018 and 2020 (Liu et al., 2023a).

4.2. *Dominant meteorological factor to variations of $PM_{2.5}$ and MDA8 O_3*

The correlations between air pollutants and meteorological conditions have been widely used to understand the role of meteorological factors on air pollutant variations (Chen et al., 2020c). It should be noted that the correlation does not imply causation and the meteorological factors are not independent of each other. Therefore, the SHAP analysis coupled with the correlations between air pollutants and meteorological conditions (Fig. S5 and Fig. S6), and long-term trends of meteorological

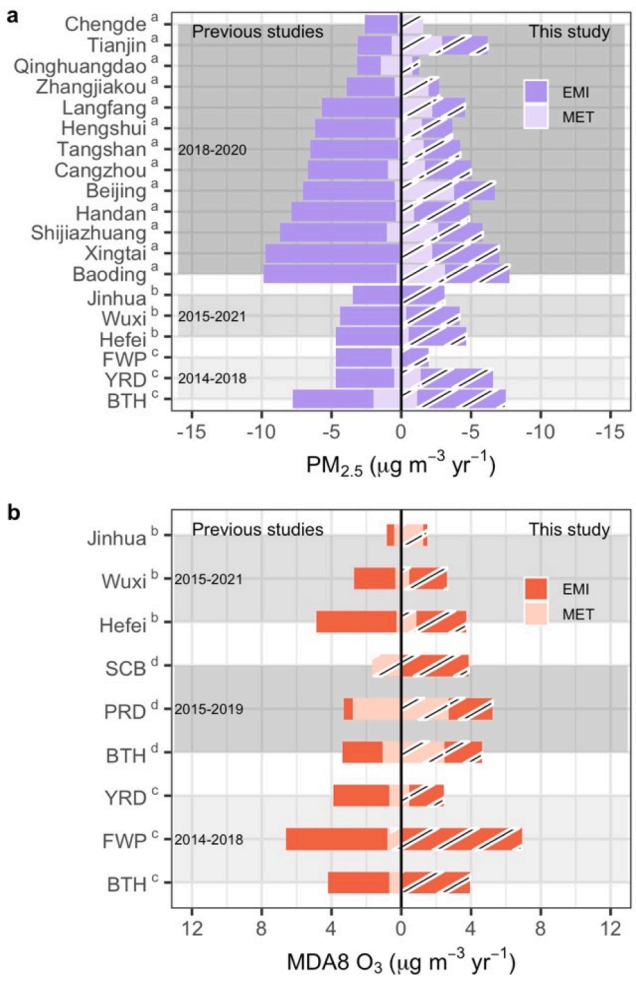

Fig. 5. Comparison of long-term, emission-related (EMI), and meteorology-related (MET) trends of $PM_{2.5}$ (a) and MDA8 O_3 (b) in this study and previous studies (a: Gao et al. (2022); b: Zhu et al. (2023); c: Chen et al., (2020b); d: Mousavinezhad et al. (2021)). The filled gray rects represent different study periods.

parameters (Fig. S7) were used to determine the dominant meteorological factor contributing to the decrease in $PM_{2.5}$ and increase in MDA8 O_3 (see Text S5 for details).

As shown in Fig. 7, the dominant meteorological condition associated with the reductions of $PM_{2.5}$ in FWP, THB, and YRD was the increase in temperature. The high temperature promotes stronger thermal activities and turbulence, resulting in better dispersion conditions for air pollutants (Chen et al., 2020c). Additionally, high temperature contributes to the loss of some $PM_{2.5}$ components such as ammonium nitrate, semi-volatile, and volatile components (Chen et al., 2020c). Therefore, the increased temperature contributed to the reduction of $PM_{2.5}$. The dominant factor in the reductions of $PM_{2.5}$ in PRD and SCB was the increased boundary layer height. A higher boundary layer height facilitates the vertical dispersion of air pollutants, leading to reduced surface $PM_{2.5}$ levels (Chen et al., 2020c). In the case of $PM_{2.5}^{MET}$ reduction in BTH, it was primarily influenced by a decrease in the northward wind component (Fig. 7a). Previous studies have indicated the haze in BTH is typically associated with the low speeds of southern wind, which brought pollutants from the south to BTH (An et al., 2019; Huang et al., 2020). As shown in Fig. S7, V10 showed a decreasing trend in BTH, suggesting less air pollutant transport from south to north.

Regarding MDA8 O_3, the increased temperature was the dominant meteorological factor contributing to the increase of MDA8 O_3 in BTH and FWP (Fig. 7a, b). The relationship between temperature and O_3 levels can be explained by the temperature-dependent mechanisms involving O_3 precursor emissions, lifetimes, and reaction rates (Lu et al., 2019; Porter and Heald, 2019). For instance, biogenic VOC and soil NO_x emissions increase with rising temperature, which further contributes to local O_3 formation (Roelle and Aneja, 2002; Ma et al., 2019b; Porter and Heald, 2019). As shown in Fig. S7, T2M in BTH and FWP showed increasing trends from 2014 to 2022, suggesting T2M contributed to O_3 increases in these two regions. It should be noted that the overall impacts of meteorological variations contributed to the decreases in O_3 in BTH and FWP, which was contrary to other regions (Section 3.2). The differences can be explained by the regional differences in trends of meteorological conditions. For instance, the negative correlation between O_3 and RH was found in six regions (Fig. S6). Therefore, the increases in RH (Fig. S7) contributed to the reductions of meteorology-related trends of MDA8 O_3 in BTH and FWP, while RH showed decreasing trends and contributed to increases in O_3 in the other four regions.

In THB and YRD, the reduction in relative humidity played a key role in the increased MDA8 O_3 levels (Fig. 7e, f). The mechanisms explaining the effects of RH on O_3 have been well summarized in the research of Li et al., (2021a). Briefly, the presence of moisture in the atmosphere hinders the formation of O_3 by reducing air temperature, shortening the chain length of peroxy radical chemical amplifiers, and decreasing the chain length of NO_2 through increased particle water. Additionally, water vapor catalytically destroys existing O_3 photochemically through the O_3 destruction cycle (Yu, 2019). Therefore, the reduction of relative humidity contributes to the enhancement of O_3. In PRD, the dominant factor for increased O_3 was the decreased total cloud cover (Fig. 7c), while in SCB, the increased boundary layer height played a major role (Fig. 7d). The higher boundary layer height contributes to the increased surface O_3 can be explained as the vertical injection of O_3 from the residual layer and downdrafts in convective storms (Caputi et al., 2019; Zhu et al., 2020; Meng et al., 2022). This phenomenon suggests that the surface O_3 variations are not only impacted by local chemical formation but also influenced by upper air concentration, which is typically linked to regional ozone background.

4.3. Achievements and challenges of air quality control in China

To protect human health from air pollution, the Chinese government launches a series of air pollution control measures since 2013 (see Text S4 for details), and air quality in China has indeed improved. In 2022, the annual mean $PM_{2.5}$ concentration in 339 cities was 29 μg m^{-3} and the non-attainment rate of air quality among these cities decreased to 37.2% (https://www.gov.cn/lianbo/bumen/202305/content_6883708.htm) according to Chinese ambient air quality standards (GB 3095-2012). As a result, health benefits are gained from the reduction of air pollutants (Zhang et al., 2019; Yang et al., 2022a; Xiao et al., 2022; Xue et al., 2023). The reduced $PM_{2.5}$-attributable excess deaths were estimated to be 0.37 million since the implementation of APPCA (Zhang et al., 2019). After the implementation of TYAP, premature deaths due to long-term $PM_{2.5}$ exposure decreased by 0.13 million from 1.52 million in 2018 to 1.39 million in 2020 (Xiao et al., 2022). The reduction of NO_2 concentrations also reduced premature deaths by 66 thousand from 2013 (316 thousand) to 2022 (250 thousand) (Xue et al., 2023). Despite the health benefits gained from the reduction of $PM_{2.5}$ and NO_2, the enhanced O_3 concentration offset the benefits. Premature deaths due to long-term O_3 exposure in China increased by 32.4 thousand from 98.9 thousand in 2013 to 131.3 thousand in 2017 and continuously increased by 13% from 2017 to 147.7 thousand in 2020 (Xiao et al., 2022). Therefore, stronger policies are required to substantially reduce deaths from air pollution in China.

Further air quality improvement in China faces three key challenges. Firstly, as air pollutant levels continue to decrease, achieving additional emission reductions becomes more difficult, particularly considering the

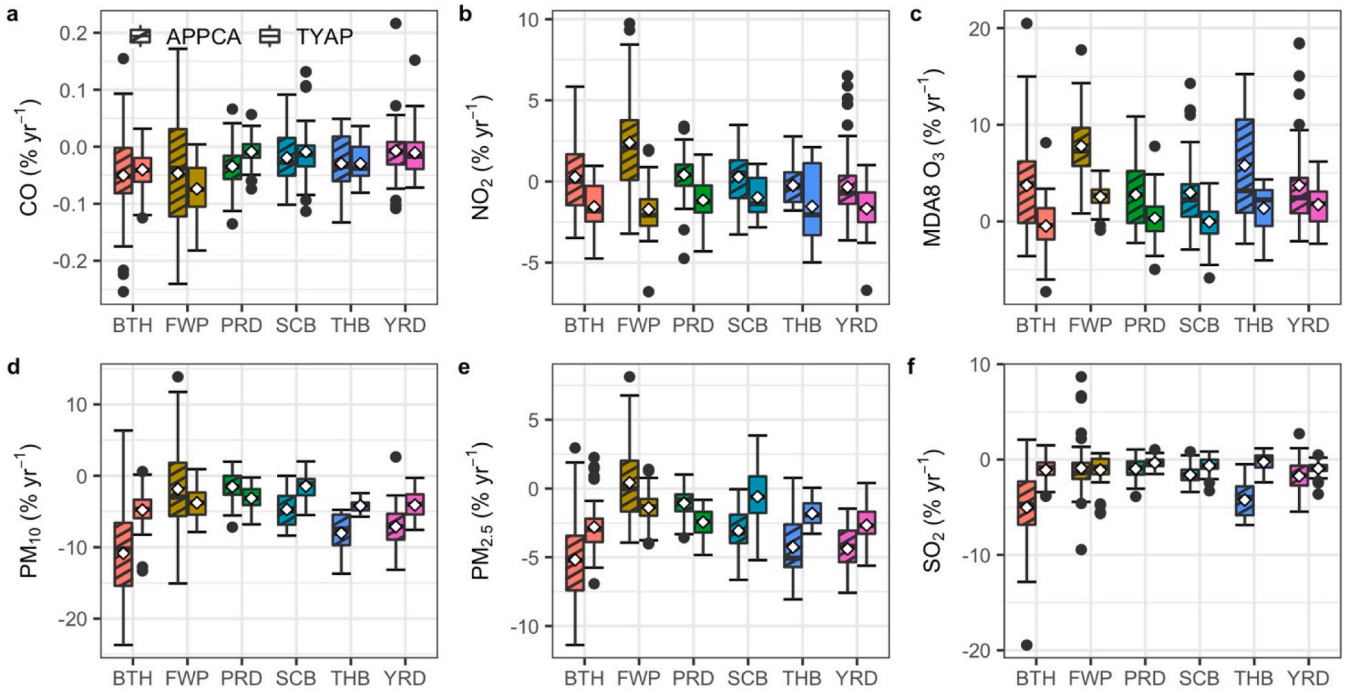

Fig. 6. Emission-related long-term trends of CO (a), NO_2 (b), MDA8 O_3 (c), PM_{10} (d), $PM_{2.5}$ (e), and SO_2 (f) during 2014–2017 (APPCA) and 2018–2020 (TYAP) in different regions.

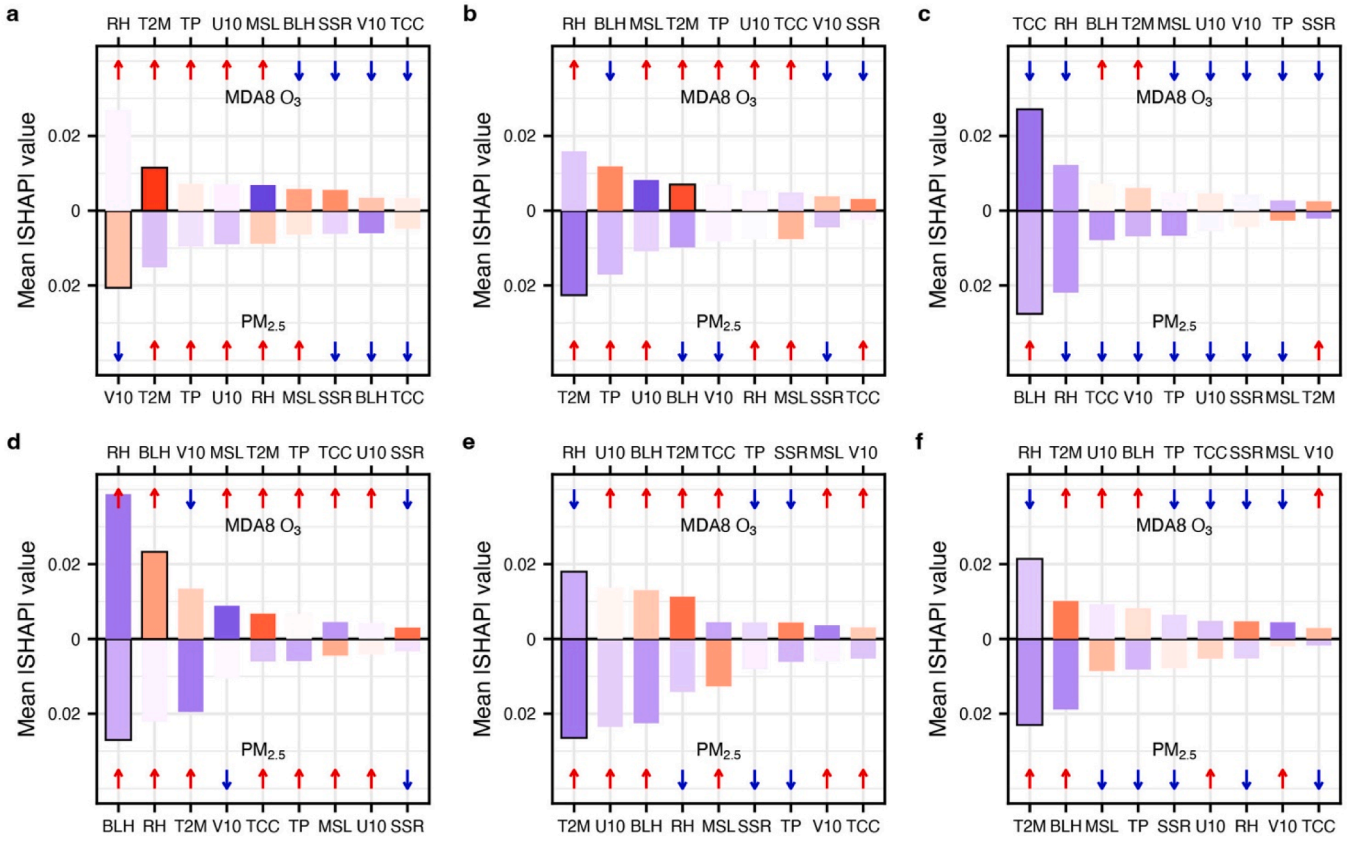

Fig. 7. The dominant meteorological factor (bar marked with black outline) contributing to the increasing trends in meteorology-related trends of MDA8 O_3 (top of each panel) and decreasing trends of $PM_{2.5}$ (bottom of each panel) in different regions including BTH (a), FWP (b), PRD (c), SCB (d), THB (e), and YRD (f). The color of the bars is mapped to the Pearson correlation coefficients($r > 0$: red; $r < 0$: blue) between air pollutants and meteorological conditions (site-specific correlations are provided in Fig. S5 and Fig. S6). The red and blue arrows represent the increasing and decreasing trends of meteorological conditions respectively (see Fig. S7 for site-specific trends). (For interpretation of the references to color in this figure legend, the reader is referred to the web version of this article.)

relatively low ambient levels of air pollutants. For instance, the BTH region had the highest average $PM_{2.5}$ level (55.4 ± 14.1 μg m^{-3}) and showed the highest decreasing trend of $PM_{2.5}$ (−5.90 μg m^{-3} yr^{-1}) during 2014–2022 among the six regions. Conversely, the PRD region, with the lowest average $PM_{2.5}$ level (27.2 ± 4.04 μg m^{-3}), demonstrated the lowest long-term variation rate of $PM_{2.5}$ (−2.02 μg m^{-3} yr^{-1}) among the six regions. Cheng et al. (2021) indicated that the benefits from end-of-pipe pollution control measures will mostly be exhausted by 2030 without ambitious climate goals. Furthermore, without significant action, the $PM_{2.5}$ levels may not meet the WHO air quality guidelines, and premature deaths resulting from $PM_{2.5}$ exposure may not consistently decrease by 2050 in China, as highlighted by Liu et al. (2022). Therefore, further drivers from systemic social-economy changes are needed. For instance, Cheng et al. (2021) suggested that China's commitment to carbon neutrality, coupled with a decrease in fossil fuel fraction to 28% (while the current fraction was 85%) in the energy structure, could result in an annual $PM_{2.5}$ level of 7.9 μg m^{-3}.

Secondly, the increasing marginal cost associated with further reducing air pollutant emissions necessitates the consideration of more targeted reduction measures for specific pollutants. Abating NH_3 emission has been proposed as a more cost-effective way to mitigate $PM_{2.5}$ air pollution in China (Bai et al., 2019; Liu et al., 2019; Gu et al., 2021; Zhai et al., 2021). As the largest NH_3 emission contributor, agricultural activities accounted for more than 80% of its emissions in China (Zhang et al., 2018b). Within the agriculture sector, NH_3 emissions from livestock predominated with a contribution of about 60% (Kang et al., 2016; Liao et al., 2022). Recent studies reveal that NH_3 emissions in Chinese cities are mainly from vehicle exhausts (Pan et al., 2016; Zhang et al., 2020; Gu et al., 2022; Wang et al., 2023). The difference in the dominant sector for NH_3 emission between rural and urban areas makes the alleviation of $PM_{2.5}$ pollution through controlling NH_3 even more complicated in China. It was estimated that the removal of NH_3 emissions from the agriculture sector could reduce the percentage of $PM_{2.5}$ mass burden by 24% to 42% in most parts of eastern China (Han et al., 2020). The initial cost to control $PM_{2.5}$ mass through NH_3 emission reduction was $140−$320 million (Zheng et al., 2019), and the total cost to reduce NH_3 emission by 50% across China was estimated as $6.6 billion (Liu et al., 2019). It should also be noted that higher NH_3 emission reduction (e.g., > 50%) would result in side effects such as aggravated precipitation acidification (Liu et al., 2019). The most cost-effective ratio for NH_3 emissions was estimated to be 20%–30% in Northern China, while the same reduction ratio would result in fewer net benefits in Southern China and SCB (Liu et al., 2019). Therefore, it is crucial to implement the most cost-effective strategy for NH_3 emission control while considering region-specific abatement strategies for NH_3 emissions.

Thirdly, coordinated control of $PM_{2.5}$ and O_3 is needed to further improve air quality in China. It was reported that a specific $PM_{2.5}$ concentration threshold existed, at which point the correlation between $PM_{2.5}$ and O_3 transitioned from negative to positive (Chu et al., 2020; Wang et al., 2023). Under the high $PM_{2.5}$ level (e.g., > 50 μg m^{-3}), the interaction between $PM_{2.5}$ and O_3 levels can be described as a "seesaw" effect, wherein decreasing $PM_{2.5}$ levels can increase O_3 concentrations (Chu et al., 2020). This phenomenon arises from the role of $PM_{2.5}$ as a sink for hydroperoxy and NO_x radicals, which would otherwise contribute to ozone production (Li et al., 2019a). Additionally, an increase in $PM_{2.5}$ can suppress O_3 through the weakened photochemical reactions resulting from less solar radiation, i.e., lower temperature, and reduced photolysis rates (Li et al., 2017; Li et al., 2019a; Sicard et al., 2023b). Aerosol chemistry is also influenced by the removal of reactive species, such as HO_x, which occur on the particle surfaces (Lou et al., 2014; Li et al., 2022). For instance, O_3 during dust events ($PM_{2.5}$ > 50 μg m^{-3}) decreased by 30% compared to the non-dusty clear-sky days over Tehran city (Sicard et al., 2023b). Under the low $PM_{2.5}$ level, there is a tendency for $PM_{2.5}$ and O_3 to be positively correlated due to their common precursors, such as VOCs and NO_x, as well as their simultaneous production in photochemical reactions. Therefore, controlling the common precursors of $PM_{2.5}$ and O_3 is needed to simultaneously solve the complex pollution of $PM_{2.5}$ and O_3 (Li et al., 2019b). Reduction of VOC and NO_x emissions to alleviate O_3 pollution, however, is highly dependent on the chemical formation regime of O_3. Reduction of VOC in a VOC-limited or reduction of NO_x in a NO_x-limited regime would reduce O_3 level, while NO_x reduction in a VOC-limited regime would increase O_3 due to less NO titration (Li et al., 2013; Jin and Holloway, 2015). Due to the non-linear response between O_3-VOC-NO_x, O_3 enhancement in the VOC-limited regime was related to NO_x emission reduction in China (Wang et al., 2019; Ren et al., 2022; Wei et al., 2022). Recently, the reduction of NO_x during COVID-19 also showed a tendency to increase O_3 at urban stations, where the O_3 formation was mostly in the VOC-limited regime, while observations at rural background stations showed the reduction of O_3 (Cristofanelli et al., 2021; Matthias et al., 2021; Steinbrecht et al., 2021). Our results showed a similar phenomenon that the station (N = 473) with the increasing trend of MDA8 O_3 also had a decreasing trend of NO_2 (Fig. 8a, b), which implied that O_3 formation in these stations was in the VOC-limited regime. Some stations (N = 26), however, showed both decreasing trends of NO_2 and MDA8 O_3, suggesting that O_3 formation was in the NO_x-limited regime. Interestingly, all of the stations with co-decreasing trends of NO_x and MDA8 O_3 showed reductions of $PM_{2.5}$ (Fig. 8c), suggesting that $PM_{2.5}$ and O_3 can be simultaneously controlled. Since the O_3 formation regime within a city shows spatial heterogeneity, which means O_3 formation in some regions is in a VOC-limited regime while the other regions are in the transition or NO_x-limited regimes (Li et al., 2021b; Yang et al., 2022b). Therefore, site-specific knowledge about atmospheric chemistry is needed to reduce the O_3 level. For instance, the ratio of 3:2, 2:3, and 3:1 co-reduction of VOC to NO_x was recommended to reduce O_3 at the NO_x-limited, VOC-limited, and transition regime sites, respectively, in Zibo city (Li et al., 2021b). To identify the O_3 chemical formation regimes at site-specific or city-scale, the ground observation-based method with model simulation (Li et al., 2021b; Yang et al., 2022b) and photochemical indicator (e.g., the ratio of formaldehyde to NO_2) based on satellite observations (Jin et al., 2020; Li et al., 2021c) are usually applied. These methods, however, have some limitations (Souri et al., 2020; Liu and Shi, 2021). A method with simple input (e.g., only observations of O_3 and NO_x) and robust results is required to evaluate the response of O_3 to reductions of VOC and NO_x, in particular, for sites and regions where local atmospheric chemistry information is unavailable. Recently, a method using the ratio of daytime-produced O_3 (DPO_3) to an 8 h-NO_2 concentration ([DPO_3]/[8 h-NO_2]) to identify the O_3 formation regime was developed, and the VOC-limited regime was identified as the [DPO_3]/[8 h-NO_2] ratio less than 8.3 (Guo et al., 2023). This method has the potential application to identify the O_3 formation regime in each air quality monitoring station and contributes to solving O_3 pollution at a station or a city scale.

5. Conclusions

This study used the Kolmogorov-Zurbenko filter coupled with multiple-linear regression to investigate the drivers of $PM_{2.5}$ and MDA8 O_3 variations in China from 2014 to 2022. The analysis revealed a reduction of 7.36 ± 2.92% yr^{-1} for $PM_{2.5}$ in China with the dominant contribution from emission reduction (85.8%). On the contrary, the MDA8 O_3 increased by 3.71 ± 2.89% yr^{-1} with less contribution from variations in meteorological conditions (14.0%). The dominant meteorological factors to the reduction of $PM_{2.5}$ and increase of MDA8 O_3 were identified as the increases in temperature, boundary layer height, and decrease in relative humidity. A comparison in emission-related trends of $PM_{2.5}$ and MDA8 O_3 between 2014–2017 and 2018–2020 showed a slower increase in MDA8 O_3 and a slower decrease in $PM_{2.5}$ during 2018–2020, suggesting that further air pollutant emission reductions would be more challenging. To further reduce the $PM_{2.5}$ levels, more targeted emission reduction measures (e.g., NH_3 emission reductions from the agriculture sector in rural areas and the transport sector in

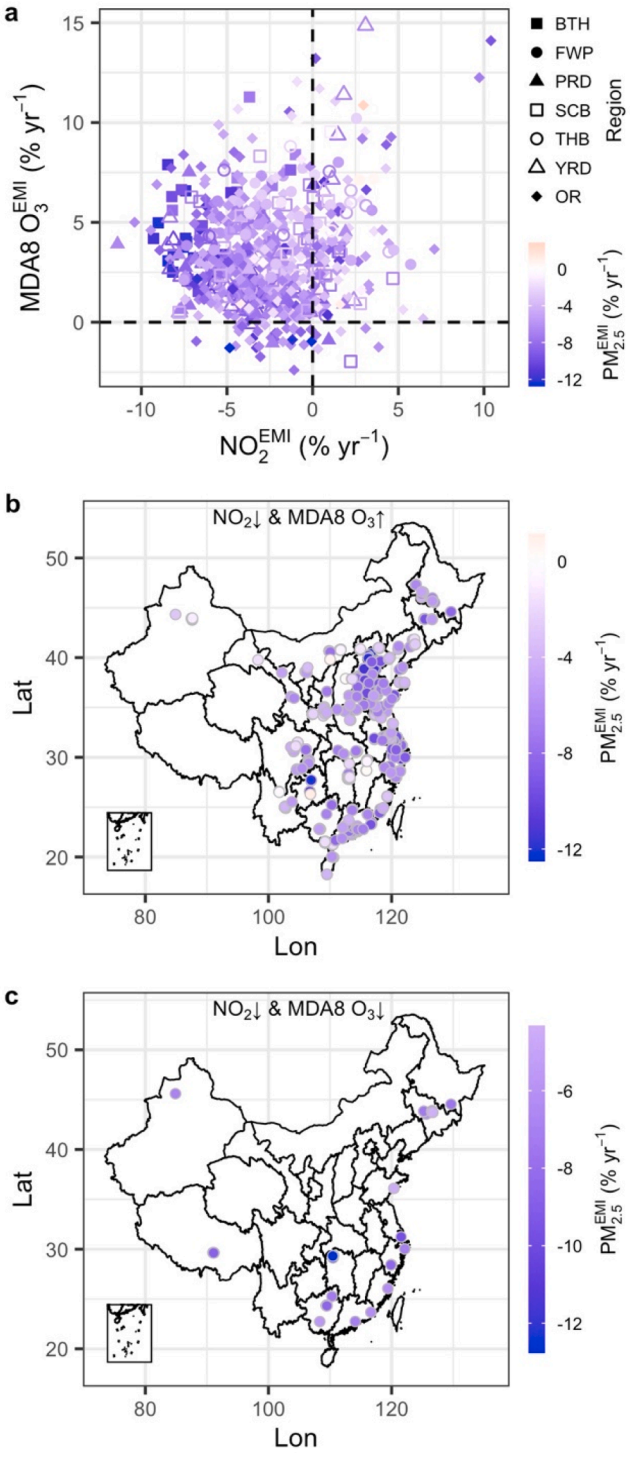

Fig. 8. Scatterplot between emission-related trends of NO_2 (NO_2^{EMI}) and MDA8 O_3 (MDA8 O_3^{EMI}) from 2014 to 2022 in China (a) and the spatial distributions of stations with decreasing trends of NO_2 while increasing trends of MDA8 O_3 (b) and co-reduction of NO_2 and MDA8 O_3 (c). The shapes of the point in panel a are mapped to six regions and other regions (OR). The colors of dots are mapped to the emission-related long-term trends of $PM_{2.5}$ ($PM_{2.5}^{EMI}$) in all panels.

urban areas) are needed. To alleviate the O_3 pollution, site-specific chemical formation regimes based on local atmospheric chemistry are needed before determining the delicate emission reduction ratios for VOC and NO_x.

CRediT authorship contribution statement

Huang Zheng: Writing – original draft, Writing – review & editing, Visualization, Methodology. **Shaofei Kong:** Conceptualization, Writing – review & editing, Supervision, Funding acquisition. **Jihoon Seo:** Methodology. **Yingying Yan:** Writing – review & editing. **Yi Cheng:** Data curation. **Liquan Yao:** Data curation. **Yanxin Wang:** Supervision. **Tianliang Zhao:** Conceptualization, Funding acquisition. **Roy M. Harrison:** Writing – review & editing, Supervision.

Declaration of Competing Interest

The authors declare that they have no known competing financial interests or personal relationships that could have appeared to influence the work reported in this paper.

Data availability

Data will be made available on request.

Acknowledgment

This study was financially supported by the National Natural Science Foundation of China (41830965) and the Key Program for Technical Innovation of Hubei Province (2017ACA089).

Appendix A. Supplementary data

Supplementary data to this article can be found online at https://doi.org/10.1016/j.envint.2023.108361.

References

An, Z., Huang, R., Zhang, R., Tie, X., Li, G., Cao, J., Zhou, W., Shi, Z., Han, Y., Gu, Z., Ji, Y., 2019. Severe haze in northern China: a synergy of anthropogenic emissions and atmospheric processes. Proc. Natl. Acad. Sci. USA 116, 8657–8666. https://doi.org/10.1073/pnas.1900125116.

Bai, Z., Winiwarter, W., Klimont, Z., Velthof, G., Misselbrook, T., Zhao, Z., Jin, X., Oenema, O., Hu, C., Ma, L., 2019. Further improvement of air quality in China needs clear ammonia mitigation target. Environ. Sci. Technol. 53, 10542–10544. https://doi.org/10.1021/acs.est.9b04725.

Brandon, G., 2023. fastshap: Fast Approximate Shapley Values. https://github.com/bgreenwell/fastshap.

Caputi, D.J., Faloona, I., Trousdell, J., Smoot, J., Falk, N., Conley, S., 2019. Residual layer ozone, mixing, and the nocturnal jet in California's San Joaquin Valley. Atmos. Chem. Phys. 19, 4721–4740. https://doi.org/10.5194/acp-19-4721-2019.

Carslaw, D.C., Ropkins, K., 2012. openair — An R package for air quality data analysis. Environ. Modell. Softw. 27–28, 52–61. https://doi.org/10.1016/j.envsoft.2011.09.008.

Chen, Z., Chen, D., Kwan, M.P., Chen, B., Gao, B., Zhuang, Y., Li, R., Xu, B., 2019. The control of anthropogenic emissions contributed to 80% of the decrease in $PM_{2.5}$ concentrations in Beijing from 2013 to 2017. Atmos. Chem. Phys. 19, 13519–13533. https://doi.org/10.5194/acp-19-13519-2019.

Chen, Q., Fu, T.M., Hu, J., Ying, Q., Zhang, L., 2017. Modelling secondary organic aerosols in China. Natl. Sci. Rev. 4, 806–809.

Chen, Z., Li, R., Chen, D., Zhuang, Y., Gao, B., Yang, L., Li, M., 2020a. Understanding the causal influence of major meteorological factors on ground ozone concentrations across China. J. Clean. Prod. 242, 118498 https://doi.org/10.1016/j.jclepro.2019.118498.

Chen, Z., Chen, D., Zhao, C., Kwan, M., Cai, J., Zhuang, Y., Zhao, B., Wang, X., Chen, B., Yang, J., Li, R., He, B., Gao, B., Wang, K., Xu, B., 2020c. Influence of meteorological conditions on $PM_{2.5}$ concentrations across China: a review of methodology and mechanism. Environ. Int. 139, 105558 https://doi.org/10.1016/j.envint.2020.105558.

Chen, L., Zhu, J., Liao, H., Yang, Y., Yue, X., 2020b. Meteorological influences on $PM_{2.5}$ and O_3 trends and associated health burden since China's clean air actions. Sci. Total Environ. 744, 140837 https://doi.org/10.1016/j.scitotenv.2020.140837.

Cheng, J., Su, J., Cui, T., Li, X., Dong, X., Sun, F., Yang, Y., Tong, D., Zheng, Y., Li, Y., Li, J., Zhang, Q., He, K., 2019. Dominant role of emission reduction in $PM_{2.5}$ air quality improvement in Beijing during 2013–2017: a model-based decomposition analysis. Atmos. Chem. Phys. 19, 6125–6146. https://doi.org/10.5194/acp-19-6125-2019.

Cheng, J., Tong, D., Zhang, Q., Liu, Y., Lei, Y., Yan, G., Yan, L., Yu, S., Cui, R.Y., Clarke, L., Geng, G., Zheng, B., Zhang, X., Davis, S.J., He, K., 2021. Pathways of China's $PM_{2.5}$ air quality 2015–2060 in the context of carbon neutrality. Natl. Sci. Rev. 8, nwab078. https://doi.org/10.1093/nsr/nwab078.

Chu, B., Ma, Q., Liu, J., Ma, J., Zhang, P., Chen, T., Feng, Q., Wang, C., Yang, N., Ma, H., Ma, J., Russell, A.G., He, H., 2020. Air pollutant correlations in China: secondary air pollutant responses to NO_x and SO_2 control. Environ. Sci. Technol. Lett. 7, 695–700. https://doi.org/10.1021/acs.estlett.0c00403.

Close, B., Zurbenko, I., Sun, M., 2018. kza: Kolmogorov-Zurbenko Adaptive Filters.

Cristofanelli, P., Arduni, J., Serva, F., Calzolari, F., Bonasoni, P., Busetto, M., Maione, M., Sprenger, M., Trisolino, P., Putero, D., 2021. Negative ozone anomalies at a high mountain site in northern Italy during 2020: a possible role of COVID-19 lockdowns? Environ. Res. Lett. 16 (7), 074029. https://doi.org/10.1088/1748-9326/ac0b6a.

Dai, X., Zhang, B., Jiang, X., Liu, L., Fang, D., Long, Z., 2022. Has the Three-Year Action Plan improved the air quality in the Fenwei Plain of China? Assessment based on a machine learning technique. Atmos. Environ. 286, 119204 https://doi.org/10.1016/j.atmosenv.2022.119204.

Dang, R., Liao, H., Fu, Y., 2021. Quantifying the anthropogenic and meteorological influences on summertime surface ozone in China over 2012–2017. Sci. Total Environ. 754, 142394 https://doi.org/10.1016/j.scitotenv.2020.142394.

Ding, A.J., Huang, X., Nie, W., Sun, J.N., Kerminen, V.M., Petäjä, T., Su, H., Cheng, Y.F., Yang, X.Q., Wang, M.H., Chi, X.G., Wang, J.P., Virkkula, A., Guo, W.D., Yuan, J., Wang, S.Y., Zhang, R.J., Wu, Y.F., Song, Y., Zhu, T., Zilitinkevich, S., Kulmala, M., Fu, C.B., 2016. Enhanced haze pollution by black carbon in megacities in China. Geophys. Res. Lett. 43, 2873–2879. https://doi.org/10.1002/2016GL067745.

Du, H., Li, J., Wang, Z., Chen, X., Yang, W., Sun, Y., Xin, J., Pan, X., Wang, W., Ye, Q., Dao, X., 2022. Assessment of the effect of meteorological and emission variations on winter $PM_{2.5}$ over the North China Plain in the three-year action plan against air pollution in 2018–2020. Atmos. Res. 280, 106395 https://doi.org/10.1016/j.atmosres.2022.106395.

Dutton, J.A., 1976. The ceaseless wind: an introduction to the theory of atmospheric motion. McGraw-Hill, New York.

Eskridge, R.E., Ku, J.Y., Rao, S.T., Porter, P.S., Zurbenko, I.G., 1997. Separating different scales of motion in time series of meteorological variables. Bull. Amer. Meteor. Soc. 78 (7), 1473–1483.

Fan, H., Zhao, C., Yang, Y., 2020. A comprehensive analysis of the spatio-temporal variation of urban air pollution in China during 2014–2018. Atmos. Environ. 220, 117066 https://doi.org/10.1016/j.atmosenv.2019.117066.

Fang, C., Qiu, J., Li, J., Wang, J., 2022. Analysis of the meteorological impact on $PM_{2.5}$ pollution in Changchun based on KZ filter and WRF-CMAQ. Atmos. Environ. 271, 118924 https://doi.org/10.1016/j.atmosenv.2021.118924.

Fiore, A.M., Naik, V., Spracklen, D.V., Steiner, A., Unger, N., Prather, M., Bergmann, D., Cameron-Smith, P.J., Cionni, I., Collins, W.J., Dalsøren, S., Eyring, V., Folberth, G.A., Ginoux, P., Horowitz, L.W., Josse, B., Lamarque, J.-F., MacKenzie, I.A., Nagashima, T., O'Connor, F.M., Righi, M., Rumbold, S.T., Shindell, D.T., Skeie, R.B., Sudo, K., Szopa, S., Takemura, T., Zeng, G., 2012. Global air quality and climate. Chem. Soc. Rev. 41, 6663–6683. https://doi.org/10.1039/C2CS35095E.

Gao, M., Han, Z., Liu, Z., Li, M., Xin, J., Tao, Z., Li, J., Kang, J.-E., Huang, K., Dong, X., Zhuang, B., Li, S., Ge, B., Wu, Q., Cheng, Y., Wang, Y., Lee, H.J., Kim, C.H., Fu, J.S., Wang, T., Chin, M., Woo, J.H., Zhang, Q., Wang, Z., Carmichael, G.R., 2018. Air quality and climate change, Topic 3 of the Model Inter-Comparison Study for Asia Phase III (MICS-Asia III) – Part 1: Overview and model evaluation. Atmos. Chem. Phys. 18, 4859–4884. https://doi.org/10.5194/acp-18-4859-2018.

Gao, S., Yu, J., Yang, W., Qu, F., Chen, L.i., Sun, Y., Zhang, H., Mao, J., Zhao, H., Azzi, M., Bai, Z., 2022. Background concentration of atmospheric $PM_{2.5}$ in the Beijing–Tianjin–Hebei urban agglomeration: levels, variation trends, and influences of meteorology and emission. Atmos. Pollut. Res. 13 (11), 101583. https://doi.org/10.1016/j.apr.2022.101583.

Geng, G., Liu, Yang, Cheng, J., Liu, Yan, Liu, Yuxi, Wu, N., Hu, H., Tong, D., Zheng, B., He, K., Zhang, Q., 2023. Contrasting emission trends between the two phases of China's clean air actions from 2013–2020. PREPRINT (Version 1) available at Research Square [https://doi.org/10.21203/rs.3.rs-2827208/v1].

Geng, G., Xiao, Q., Zheng, Y., Tong, D., Zhang, Y., Zhang, X., Zhang, Q., He, K., Liu, Y., 2019. Impact of China's Air Pollution Prevention and Control Action Plan on $PM_{2.5}$ chemical composition over eastern China. Sci. China Earth Sci. 62, 1872–1884. https://doi.org/10.1007/s11430-018-9353-x.

Grange, S.K., Carslaw, D.C., Lewis, A.C., Boleti, E., Hueglin, C., 2018. Random forest meteorological normalisation models for Swiss PM_{10} trend analysis. Atmos. Chem. Phys. 18, 6223–6239. https://doi.org/10.5194/acp-18-6223-2018.

Grange, S.K., Carslaw, D.C., 2019. Using meteorological normalisation to detect interventions in air quality time series. Sci. Total Environ. 653, 578–588. https://doi.org/10.1016/j.scitotenv.2018.10.344.

Gu, M., Pan, Y., Walters, W.W., Sun, Q., Song, L., Wang, Y., Xue, Y., Fang, Y., 2022. Vehicular emissions enhanced ammonia concentrations in winter mornings: insights from diurnal nitrogen isotopic signatures. Environ. Sci. Technol. 56, 1578–1585. https://doi.org/10.1021/acs.est.1c05884.

Gu, B., Zhang, L., Van Dingenen, R., Vieno, M., Van Grinsven, H.J., Zhang, X., Zhang, S., Chen, Y., Wang, S., Ren, C., Rao, S., Holland, M., Winiwarter, W., Chen, D., Xu, J., Sutton, M.A., 2021. Abating ammonia is more cost-effective than nitrogen oxides for mitigating $PM_{2.5}$ air pollution. Science 374, 758–762. https://doi.org/10.1126/science.abf8623.

Guo, J., Zhang, X., Gao, Y., Wang, Z., Zhang, M., Xue, W., Herrmann, H., Brasseur, G.P., Wang, T., Wang, Z., 2023. Evolution of ozone pollution in China: what track will It follow? Environ. Sci. Technol. 57, 109–117. https://doi.org/10.1021/acs.est.2c08205.

Hadley, W., 2016. Ggplot2. Springer Science+Business Media, LLC, New York, NY.

Hallquist, M., Munthe, J., Hu, M., Wang, T., Chan, C.K., Gao, J., Boman, J., Guo, S., Hallquist, Å.M., Mellqvist, J., Moldanova, J., Pathak, R.K., Pettersson, J.BC., Pleijel, H., Simpson, D., Thynell, M., 2016. Photochemical smog in China: scientific challenges and implications for air-quality policies. Natl. Sci. Rev. 3 (4), 401–403. https://doi.org/10.1093/nsr/nww080.

Han, X., Zhu, L., Liu, M., Song, Y., Zhang, M., 2020. Numerical analysis of agricultural emissions impacts on $PM_{2.5}$ in China using a high-resolution ammonia emission inventory. Atmos. Chem. Phys. 20, 9979–9996. https://doi.org/10.5194/acp-20-9979-2020.

Hersbach, H., Bell, B., Berrisford, P., Biavati, G., Horányi, A., Muñoz Sabater, Nicolas, J., Peubey, C., Radu, R., Rozum, I., Schepers, D., Simmons, A., Soci, C., Dee, D., Thépaut, J.N., 2023. ERA5 hourly data on single levels from 1940 to present. Copernicus Climate Change Service (C3S) Climate Data Store (CDS). https://doi.org/10.24381/cds.adbb2d47.

Huang, X., Ding, A., Wang, Z., Ding, K., Gao, J., Chai, F., Fu, C., 2020. Amplified transboundary transport of haze by aerosol–boundary layer interaction in China. Nat. Geosci. 13, 428–434. https://doi.org/10.1038/s41561-020-0583-4.

Huang, J., Pan, X., Guo, X., Li, G., 2018. Health impact of China's Air Pollution Prevention and Control Action Plan: an analysis of national air quality monitoring and mortality data. Lancet Planet. Health 2, e313–e323. https://doi.org/10.1016/S2542-5196(18)30141-4.

Huang, R., Zhang, Y., Bozzetti, C., Ho, K.F., Cao, J., Han, Y., Daellenbach, K.R., Slowik, J. G., Platt, S.M., Canonaco, F., Zotter, P., Wolf, R., Pieber, S.M., Bruns, E.A., Crippa, M., Ciarelli, G., Piazzalunga, A., Schwikowski, M., Abbaszade, G., Schnelle-Kreis, J., Zimmermann, R., An, Z., Szidat, S., Baltensperger, U., Haddad, I.E., Prévôt, A.S.H., 2014. High secondary aerosol contribution to particulate pollution during haze events in China. Nature 514, 218–222. https://doi.org/10.1038/nature13774.

Ji, Y., Zhang, Y., Liu, D., Zhang, K., Cai, P., Zhu, B., Zhang, B., Xian, J., Wang, H., Ge, X., 2023. Using machine learning to quantify drivers of aerosol pollution trend in China from 2015 to 2022. Appl. Geochem. 151, 105614 https://doi.org/10.1016/j.apgeochem.2023.105614.

Jin, X., Holloway, T., 2015. Spatial and temporal variability of ozone sensitivity over China observed from the Ozone Monitoring Instrument. J. Geophys. Res. Atmos. 120, 7229–7246. https://doi.org/10.1002/2015JD023250.

Jin, X., Fiore, A., Boersma, K.F., Smedt, I.D., Valin, L., 2020. Inferring changes in summertime surface Ozone–NO_x–VOC chemistry over U.S. urban areas from two decades of satellite and ground-based observations. Environ. Sci. Technol. 54, 6518–6529. https://doi.org/10.1021/acs.est.9b07785.

Kan, H., Chen, R., Tong, S., 2012. Ambient air pollution, climate change, and population health in China. Environ. Int. 42, 10–19. https://doi.org/10.1016/j.envint.2011.03.003.

Kang, Y., Liu, M., Song, Y., Huang, X., Yao, H., Cai, X., Zhang, H., Kang, L., Liu, X., Yan, X., He, H., Zhang, Q., Shao, M., Zhu, T., 2016. High-resolution ammonia emissions inventories in China from 1980 to 2012. Atmos. Chem. Phys. 16, 2043–2058. https://doi.org/10.5194/acp-16-2043-2016.

Li, K., Jacob, D.J., Liao, H., Shen, L., Zhang, Q., Bates, K.H., 2019a. Anthropogenic drivers of 2013–2017 trends in summer surface ozone in China. Proc. Natl. Acad. Sci. u.s.a. 116, 422–427. https://doi.org/10.1073/pnas.1812168116.

Li, K., Jacob, D.J., Liao, H., Zhu, J., Shah, V., Shen, L., Bates, K.H., Zhang, Q., Zhai, S., 2019b. A two-pollutant strategy for improving ozone and particulate air quality in China. Nat. Geosci. 12, 906–910. https://doi.org/10.1038/s41561-019-0464-x.

Li, K., Jacob, D.J., Shen, L., Lu, X., De Smedt, I., Liao, H., 2020. Increases in surface ozone pollution in China from 2013 to 2019: anthropogenic and meteorological influences. Atmos. Chem. Phys. 20, 11423–11433. https://doi.org/10.5194/acp-20-11423-2020.

Li, Y., Lau, A.K.H., Fung, J.C.H., Zheng, J., Liu, S., 2013. Importance of NO_x control for peak ozone reduction in the Pearl River Delta region. J. Geophys. Res. Atmos. 118, 9428–9443. https://doi.org/10.1002/jgrd.50659.

Li, M., Wang, T., Xie, M., Zhuang, B., Li, S., Han, Y., Chen, P., 2017. Impacts of aerosol-radiation feedback on local air quality during a severe haze episode in Nanjing megacity, eastern China. Tellus B Chem. Phys. Meteorol. 69, 1339548. https://doi.org/10.1080/16000889.2017.1339548.

Li, K., Wang, X., Li, L., Wang, J., Liu, Y., Cheng, X., Xu, B., Wang, X., Yan, P., Li, S., Geng, C., Yang, W., Azzi, M., Bai, Z., 2021b. Large variability of O_3-precursor relationship during severe ozone polluted period in an industry-driven cluster city (Zibo) of North China Plain. J. Clean. Prod. 316, 128252 https://doi.org/10.1016/j.jclepro.2021.128252.

Li, D., Wang, S., Xue, R., Zhu, J., Zhang, S., Sun, Z., Zhou, B., 2021c. OMI-observed HCHO in Shanghai, China, during 2010–2019 and ozone sensitivity inferred by an improved HCHO/NO_2 ratio. Atmos. Chem. Phys. 21, 15447–15460. https://doi.org/10.5194/acp-21-15447-2021.

Li, M., Yu, S., Chen, X., Li, Z., Zhang, Y., Wang, L., Liu, W., Li, P., Lichtfouse, E., Rosenfeld, D., Seinfeld, J.H., 2021a. Large scale control of surface ozone by relative humidity observed during warm seasons in China. Environ. Chem. Lett. 19, 3981–3989. https://doi.org/10.1007/s10311-021-01265-0.

Li, C., Zhu, Q., Jin, X., Cohen, R.C., 2022. Elucidating Contributions of Anthropogenic Volatile Organic Compounds and Particulate Matter to Ozone Trends over China. Environ. Sci. Technol. 56, 12906–12916. https://doi.org/10.1021/acs.est.2c03315.

Liang, X., Li, S., Zhang, S., Huang, H., Chen, S.X., 2016. $PM_{2.5}$ data reliability, consistency, and air quality assessment in five Chinese cities. J. Geophys. Res. Atmos. 121, 10220–10236. https://doi.org/10.1002/2016JD024877.

Liao, W., Liu, M., Huang, X., Wang, T., Xu, Z., Shang, F., Song, Y., Cai, X., Zhang, H., Kang, L., Zhu, T., 2022. Estimation for ammonia emissions at county level in China from 2013 to 2018. Sci. China Earth Sci. 65, 1116–1127. https://doi.org/10.1007/s11430-021-9897-3.

Lin, Y., Zhang, L., Fan, Q., Meng, H., Gao, Y., Gao, H., Yao, X., 2022. Decoupling impacts of weather conditions on interannual variations in concentrations of criteria air pollutants in South China – constraining analysis uncertainties by using multiple

analysis tools. Atmos. Chem. Phys. 22, 16073–16090. https://doi.org/10.5194/acp-22-16073-2022.
Liu, M., Huang, X., Song, Y., Tang, J., Cao, J., Zhang, X., Zhang, Q., Wang, S., Xu, T., Kang, L., Cai, X., Zhang, H., Yang, F., Wang, H., Yu, J.Z., Lau, A.K.H., He, L., Huang, X., Duan, L., Ding, A., Xue, L., Gao, J., Liu, B., Zhu, T., 2019. Ammonia emission control in China would mitigate haze pollution and nitrogen deposition, but worsen acid rain. Proc. Natl. Acad. Sci. u.s.a. 116, 7760–7765. https://doi.org/10.1073/pnas.1814880116.
Liu, C., Shi, K., 2021. A review on methodology in O_3-NO_x-VOC sensitivity study. Environ. Pollut. 291, 118249 https://doi.org/10.1016/j.envpol.2021.118249.
Liu, Y., Tong, D., Cheng, J., Davis, S.J., Yu, S., Yarlagadda, B., Clarke, L.E., Brauer, M., Cohen, A.J., Kan, H., Xue, T., Zhang, Q., 2022. Role of climate goals and clean-air policies on reducing future air pollution deaths in China: a modelling study. Lancet Planet. Health 6, e92–e99. https://doi.org/10.1016/S2542-5196(21)00326-0.
Liu, Y., Geng, G., Cheng, J., Liu, Y., Xiao, Q., Liu, L., Shi, Q., Tong, D., He, K., Zhang, Q., 2023a. Drivers of increasing ozone during the two phases of clean air actions in China 2013–2020. Environ. Sci. Technol. 57 (24), 8954–8964. https://doi.org/10.1021/acs.est.3c00054.
Lou, S., Liao, H., Zhu, B., 2014. Impacts of aerosols on surface-layer ozone concentrations in China through heterogeneous reactions and changes in photolysis rates. Atmos. Environ. 85, 123–138. https://doi.org/10.1016/j.atmosenv.2013.12.004.
Lu, X., Zhang, L., Shen, L., 2019. Meteorology and climate influences on tropospheric ozone: a review of natural sources, chemistry, and transport patterns. Curr. Pollut. Rep. 5, 238–260. https://doi.org/10.1007/s40726-019-00118-3.
Lundberg, S.M., Lee, S.-I., 2017. A Unified Approach to Interpreting Model Predictions. In: Guyon, I., Luxburg, U., Bengio, S., Wallach, H., Fergus, R., Vishwanathan, S., Garnett, R. (Eds.), ADVANCES IN NEURAL INFORMATION PROCESSING SYSTEMS 30 (NIPS 2017). Advances in Neural Information Processing Systems.
Ma, M., Gao, Y., Wang, Y., Zhang, S., Leung, L.R., Liu, C., Wang, S., Zhao, B., Chang, X., Su, H., Zhang, T., Sheng, L., Yao, X., Gao, H., 2019b. Substantial ozone enhancement over the North China Plain from increased biogenic emissions due to heat waves and land cover in summer 2017. Atmos. Chem. Phys. 19, 12195–12207. https://doi.org/10.5194/acp-19-12195-2019.
Ma, Z., Liu, R., Liu, Y., Bi, J., 2019a. Effects of air pollution control policies on $PM_{2.5}$ pollution improvement in China from 2005 to 2017: a satellite-based perspective. Atmos. Chem. Phys. 19, 6861–6877. https://doi.org/10.5194/acp-19-6861-2019.
Ma, Y., Ye, J., Xin, J., Zhang, W., Vilà-Guerau de Arellano, J., Wang, S., Zhao, D., Dai, L., Ma, Y., Wu, X., Xia, X., Tang, G., Wang, Y., Shen, P., Lei, Y., Martin, S.T., 2020. The stove, dome, and umbrella effects of atmospheric aerosol on the development of the planetary boundary layer in hazy regions. Geophys. Res. Lett. 47 https://doi.org/10.1029/2020GL087373.
Maji, K.J., Li, V.O., Lam, J.C., 2020. Effects of China's current Air Pollution Prevention and Control Action Plan on air pollution patterns, health risks and mortalities in Beijing 2014–2018. Chemosphere 260, 127572. https://doi.org/10.1016/j.chemosphere.2020.127572.
Mao, Y.H., Liao, H., Han, Y., Cao, J., 2016. Impacts of meteorological parameters and emissions on decadal and interannual variations of black carbon in China for 1980–2010. J. Geophys. Res. Atmos. 121, 1822–1843. https://doi.org/10.1002/2015JD024019.
Matthias, V., Quante, M., Arndt, J.A., Badeke, R., Fink, L., Petrik, R., Feldner, J., Schwarzkopf, D., Link, E.-M., Ramacher, M.O.P., Wedemann, R., 2021. The role of emission reductions and the meteorological situation for air quality improvements during the COVID-19 lockdown period in central Europe. Atmos. Chem. Phys. 21, 13931–13971. https://doi.org/10.5194/acp-21-13931-2021.
Meng, K., Zhao, T., Xu, X., Zhang, Z., Bai, Y., Hu, Y., Zhao, Y., Zhang, X., Xin, Y., 2022. Influence of stratosphere-to-troposphere transport on summertime surface O_3 changes in North China Plain in 2019. Atmos. Res. 276, 106271 https://doi.org/10.1016/j.atmosres.2022.106271.
Mousavinezhad, S., Choi, Y., Pouyaei, A., Ghahremanloo, M., Nelson, D.L., 2021. A comprehensive investigation of surface ozone pollution in China, 2015–2019: separating the contributions from meteorology and precursor emissions. Atmos. Res. 257, 105599 https://doi.org/10.1016/j.atmosres.2021.105599.
Pan, Y., Tian, S., Liu, D., Fang, Y., Zhu, X., Zhang, Q., Zheng, B., Michalski, G., Wang, Y., 2016. Fossil fuel combustion-related emissions dominate atmospheric ammonia sources during severe haze episodes: evidence from ^{15}N-stable isotope in size-resolved aerosol ammonium. Environ. Sci. Technol. 50, 8049–8056. https://doi.org/10.1021/acs.est.6b00634.
Porter, W.C., Heald, C.L., 2019. The mechanisms and meteorological drivers of the summertime ozone–temperature relationship. Atmos. Chem. Phys. 19, 13367–13381. https://doi.org/10.5194/acp-19-13367-2019.
Qiu, M., Zigler, C., Selin, N.E., 2022. Statistical and machine learning methods for evaluating trends in air quality under changing meteorological conditions. Atmos. Chem. Phys. 22 (16), 10551–10566. https://doi.org/10.5194/acp-22-10551-2022.
R Core Team, 2023. R: a language and environment for statistical computing. R Foundation for Statistical Computing, Vienna, Austria.
Rao, S.T., Zurbenko, I.G., 1994. Detecting and tracking changes in ozone air quality. J. Air. Waste. Mange. 44, 1089–1092. https://doi.org/10.1080/10473289.1994.10467303.
Rao, S.T., Zalewsky, E., Zurbenko, I.G., 1995. Determining temporal and spatial variations in ozone air quality. J. Air. Waste. Mange. 45, 57–61. https://doi.org/10.1080/10473289.1995.10467342.
Rao, S.T., Zurbenko, I.G., Neagu, R., Porter, P.S., Ku, J.Y., Henry, R.F., 1997. Space and time scales in ambient ozone data. Bull. Amer. Meteor. Soc. 78, 2153–2166. https://doi.org/10.1175/1520-0477(1997)078<2153:SATSIA>2.0.CO;2.
Ren, J., Guo, F., Xie, S., 2022. Diagnosing ozone–NO_x–VOC sensitivity and revealing causes of ozone increases in China based on 2013–2021 satellite retrievals. Atmos. Chem. Phys. 22, 15035–15047. https://doi.org/10.5194/acp-22-15035-2022.
Roelle, P.A., Aneja, V.P., 2002. Nitric oxide emissions from soils amended with municipal waste biosolids. Atmos. Environ. 36, 137–147. https://doi.org/10.1016/S1352-2310(01)00415-0.
Seo, J., Park, D.-S.-R., Kim, J.Y., Youn, D., Lim, Y.B., Kim, Y., 2018. Effects of meteorology and emissions on urban air quality: a quantitative statistical approach to long-term records (1999–2016) in Seoul, South Korea. Atmos. Chem. Phys. 18, 16121–16137. https://doi.org/10.5194/acp-18-16121-2018.
Shen, L., Zhao, T., Liu, J., Wang, H., Bai, Y., 2023. Meteorological impacts on interannual anomalies of O_3 import over Twain-Hu Basin. Sci. Total Environ. 888, 164065 https://doi.org/10.1016/j.scitotenv.2023.164065.
Shi, Z., Song, C., Liu, B., Lu, G., Xu, J., Van Vu, T., Elliott, R.J.R., Li, W., Bloss, W.J., Harrison, R.M., 2021. Abrupt but smaller than expected changes in surface air quality attributable to COVID-19 lockdowns. Sci. Adv. 7, eabd6696. https://doi.org/10.1126/sciadv.abd6696.
Shiraiwa, M., Ueda, K., Pozzer, A., Lammel, G., Kampf, C.J., Fushimi, A., Enami, S., Arangio, A.M., Fröhlich-Nowoisky, J., Fujitani, Y., Furuyama, A., Lakey, P.S.J., Lelieveld, J., Lucas, K., Morino, Y., Pöschl, U., Takahama, S., Takami, A., Tong, H., Weber, B., Yoshino, A., Sato, K., 2017. Aerosol health effects from molecular to global scales. Environ. Sci. Technol. 51, 13545–13567. https://doi.org/10.1021/acs.est.7b04417.
Sicard, P., Agathokleous, E., Anenberg, S.C., De Marco, A., Paoletti, E., Calatayud, V., 2023a. Trends in urban air pollution over the last two decades: A global perspective. Sci. Total Environ. 858, 160064 https://doi.org/10.1016/j.scitotenv.2022.160064.
Sicard, P., Khaniabadi, Y.O., Leca, S., De Marco, A., 2023b. Relationships between ozone and particles during air pollution episodes in arid continental climate. Atmos. Pollut. Res. 14 (8), 101838. https://doi.org/10.1016/j.apr.2023.101838.
Silver, B., Reddington, C.L., Arnold, S.R., Spracklen, D.V., 2018. Substantial changes in air pollution across China during 2015–2017. Environ. Res. Lett. 13, 114012 https://doi.org/10.1088/1748-9326/aae718.
Sokhi, R.S., Singh, V., Querol, X., Finardi, S., Targino, A.C., Andrade, M.d.F., Pavlovic, R., Garland, R.M., Massagué, J., Kong, S., Baklanov, A., Ren, L.u., Tarasova, O., Carmichael, G., Peuch, V.-H., Anand, V., Arbilla, G., Badali, K., Beig, G., Belalcazar, L.C., Bolignano, A., Brimblecombe, P., Camacho, P., Casallas, A., Charland, J.-P., Choi, J., Chourdakis, E., Coll, I., Collins, M., Cyrys, J., da Silva, C.M., Di Giosa, A.D., Di Leo, A., Ferro, C., Gavidia-Calderon, M., Gayen, A., Ginzburg, A., Godefroy, F., Gonzalez, Y.A., Guevara-Luna, M., Haque, S.M., Havenga, H., Herod, D., Hõrrak, U., Hussein, T., Ibarra, S., Jaimes, M., Kaasik, M., Khaiwal, R., Kim, J., Kousa, A., Kukkonen, J., Kulmala, M., Kuula, J., La Violette, N., Lanzani, G., Liu, X.i., MacDougall, S., Manseau, P.M., Marchegiani, G., McDonald, B., Mishra, S. V., Molina, L.T., Mooibroek, D., Mor, S., Moussiopoulos, N., Murena, F., Niemi, J.V., Noe, S., Nogueira, T., Norman, M., Pérez-Camaño, J.L., Petäjä, T., Piketh, S., Rathod, A., Reid, K., Retama, A., Rivera, O., Rojas, N.Y., Rojas-Quincho, J.P., San José, R., Sánchez, O., Seguel, R.J., Sillanpää, S., Su, Y., Tapper, N., Terrazas, A., Timonen, H., Toscano, D., Tsegas, G., Velders, G.J.M., Vlachokostas, C., von Schneidemesser, E., Vpm, R., Yadav, R., Zalakeviciute, R., Zavala, M., 2021. A global observational analysis to understand changes in air quality during exceptionally low anthropogenic emission conditions. Environ. Int. 157, 106818. https://doi.org/10.1016/j.envint.2021.106818.
Song, C., Wu, L., Xie, Y., He, J., Chen, X., Wang, T., Lin, Y., Jin, T., Wang, A., Liu, Y., Dai, Q., Liu, B., Wang, Y., Mao, H., 2017. Air pollution in China: status and spatiotemporal variations. Environ. Pollut. 227, 334–347. https://doi.org/10.1016/j.envpol.2017.04.075.
Souri, A.H., Nowlan, C.R., Wolfe, G.M., Lamsal, L.N., Chan Miller, C.E., Abad, G.G., Janz, S.J., Fried, A., Blake, D.R., Weinheimer, A.J., Diskin, G.S., Liu, X., Chance, K., 2020. Revisiting the effectiveness of $HCHO/NO_2$ ratios for inferring ozone sensitivity to its precursors using high resolution airborne remote sensing observations in a high ozone episode during the KORUS-AQ campaign. Atmos. Environ. 224, 117341 https://doi.org/10.1016/j.atmosenv.2020.117341.
Steinbrecht, W., Kubistin, D., Plass-Dülmer, C., Davies, J., Tarasick, D.W., von der Gathen, P., Deckelmann, H., Jepsen, N., Kivi, R., Lyall, N., Palm, M., Notholt, J., Kois, B., Oelsner, P., Allaart, M., Piters, A., Gill, M., Van Malderen, R., Delcloo, A.W., Sussmann, R., Mahieu, E., Servais, C., Romanens, G., Stübi, R., Ancellet, G., Godin-Beekmann, S., Yamanouchi, S., Strong, K., Johnson, B., Cullis, P., Petropavlovskikh, I., Hannigan, J.W., Hernandez, J.-L., Diaz Rodriguez, A., Nakano, T., Chouza, F., Leblanc, T., Torres, C., Garcia, O., Röhling, A.N., Schneider, M., Blumenstock, T., Tully, M., Paton-Walsh, C., Jones, N., Querel, R., Strahan, S., Stauffer, R.M., Thompson, A.M., Inness, A., Engelen, R., Chang, K.-L., Cooper, O.R., 2021. COVID-19 Crisis Reduces Free Tropospheric Ozone Across the Northern Hemisphere. Geophys. Res. Lett. 48 (5) https://doi.org/10.1029/2020GL091987.
Stirnberg, R., Cermak, J., Kotthaus, S., Haeffelin, M., Andersen, H., Fuchs, J., Kim, M., Petit, J.E., Favez, O., 2021. Meteorology-driven variability of air pollution PM_1 revealed with explainable machine learning. Atmos. Chem. Phys. 21, 3919–3948. https://doi.org/10.5194/acp-21-3919-2021.
Sun, L., Xue, L., Wang, Y., Li, L., Lin, J., Ni, R., Yan, Y., Chen, L., Li, J., Zhang, Q., Wang, W., 2019. Impacts of meteorology and emissions on summertime surface ozone increases over central eastern China between 2003 and 2015. Atmos. Chem. Phys. 19, 1455–1469. https://doi.org/10.5194/acp-19-1455-2019.
Sun, X., Zhao, T., Bai, Y., Kong, S., Zheng, H., Hu, W., Ma, X., Xiong, J., 2022. Meteorology impact on $PM_{2.5}$ change over a receptor region in the regional transport of air pollutants: observational study of recent emission reductions in central China. Atmos. Chem. Phys. 22, 3579–3593. https://doi.org/10.5194/acp-22-3579-2022.

von Schneidemesser, E., Monks, P.S., Allan, J.D., Bruhwiler, L., Forster, P., Fowler, D., Lauer, A., Morgan, W.T., Paasonen, P., Righi, M., Sindelarova, K., Sutton, M.A., 2015. Chemistry and the linkages between air quality and climate change. Chem. Rev. 115, 3856–3897. https://doi.org/10.1021/acs.chemrev.5b00089.

Vu, T.V., Shi, Z., Cheng, J., Zhang, Q., He, K., Wang, S., Harrison, R.M., 2019. Assessing the impact of clean air action on air quality trends in Beijing using a machine learning technique. Atmos. Chem. Phys. 19, 11303–11314. https://doi.org/10.5194/acp-19-11303-2019.

Wang, Z., Huang, X., Ding, A., 2018. Dome effect of black carbon and its key influencing factors: a one-dimensional modelling study. Atmos. Chem. Phys. 18, 2821–2834. https://doi.org/10.5194/acp-18-2821-2018.

Wang, N., Lyu, X., Deng, X., Huang, X., Jiang, F., Ding, A., 2019. Aggravating O_3 pollution due to NO_x emission control in eastern China. Sci. Total Environ. 677, 732–744. https://doi.org/10.1016/j.scitotenv.2019.04.388.

Wang, L., Zhao, B., Zhang, Y., Hu, H., 2023. Correlation between surface $PM_{2.5}$ and O_3in eastern China during 2015–2019: Spatiotemporal variations and meteorological impacts. Atmos. Environ. 294, 119520 https://doi.org/10.1016/j.atmosenv.2022.119520.

Wei, W., Wang, X., Wang, X., Li, R., Zhou, C., Cheng, S., 2022. Attenuated sensitivity of ozone to precursors in Beijing–Tianjin–Hebei region with the continuous NO_x reduction within 2014–2018. Sci. Total Environ. 813, 152589 https://doi.org/10.1016/j.scitotenv.2021.152589.

WHO global air quality guidelines: particulate matter ($PM_{2.5}$ and PM_{10}), ozone, nitrogen dioxide, sulfur dioxide and carbon monoxide: executive summary. Geneva.

Xiao, Q., Geng, G., Xue, T., Liu, S., Cai, C., He, K., Zhang, Q., 2022. Tracking $PM_{2.5}$ and O_3 pollution and the related health burden in China 2013–2020. Environ. Sci. Technol. 56, 6922–6932. https://doi.org/10.1021/acs.est.1c04548.

Xue, T., Liu, J., Zhang, Q., Geng, G., Zheng, Y., Tong, D., Liu, Z., Guan, D., Bo, Y., Zhu, T., He, K., Hao, J., 2019. Rapid improvement of $PM_{2.5}$ pollution and associated health benefits in China during 2013–2017. Sci. China Earth Sci. 62, 1847–1856. https://doi.org/10.1007/s11430-018-9348-2.

Xue, T., Tong, M., Wang, M., Yang, X., Wang, Y., Lin, H., Liu, H., Li, J., Huang, C., Meng, X., Zheng, Y., Tong, D., Gong, J., Zhang, S., Zhu, T., 2023. Health impacts of long-term NO_2 exposure and inequalities among the Chinese population from 2013 to 2020. Environ. Sci. Technol. 57, 5349–5357. https://doi.org/10.1021/acs.est.2c08022.

Yan, Y., Lin, J., Kuang, Y., Yang, D., Zhang, L., 2014. Tropospheric carbon monoxide over the Pacific during HIPPO: two-way coupled simulation of GEOS-Chem and its multiple nested models. Atmos. Chem. Phys. 14, 12649–12663. https://doi.org/10.5194/acp-14-12649-2014.

Yan, Y., Lin, J., Chen, J., Hu, L., 2016. Improved simulation of tropospheric ozone by a global-multi-regional two-way coupling model system. Atmos. Chem. Phys. 16, 2381–2400. https://doi.org/10.5194/acp-16-2381-2016.

Yan, Y., Cabrera-Perez, D., Lin, J., Pozzer, A., Hu, L., Millet, D.B., Porter, W.C., Lelieveld, J., 2019. Global tropospheric effects of aromatic chemistry with the SAPRC-11 mechanism implemented in GEOS-Chem version 9–02. Geosci. Model Dev. 12, 111–130. https://doi.org/10.5194/gmd-12-111-2019.

Yang, J., Ma, J., Sun, Q., Han, C., Guo, Y., Li, M., 2022a. Health benefits by attaining the new WHO air quality guideline targets in China: a nationwide analysis. Environ. Pollut. 308, 119694 https://doi.org/10.1016/j.envpol.2022.119694.

Yang, S., Yuan, B., Peng, Y., Huang, S., Chen, W., Hu, W., Pei, C., Zhou, J., Parrish, D.D., Wang, W., He, X., Cheng, C., Li, X.-B., Yang, X., Song, Y., Wang, H., Qi, J., Wang, B., Wang, C., Wang, C., Wang, Z., Li, T., Zheng, E., Wang, S., Wu, C., Cai, M., Ye, C., Song, W., Cheng, P., Chen, D., Wang, X., Zhang, Z., Wang, X., Zheng, J., Shao, M., 2022b. The formation and mitigation of nitrate pollution: comparison between urban and suburban environments. Atmos. Chem. Phys. 22, 4539–4556. https://doi.org/10.5194/acp-22-4539-2022.

Yin, H., Lu, X., Sun, Y., Li, K.e., Gao, M., Zheng, B.o., Liu, C., 2021. Unprecedented decline in summertime surface ozone over eastern China in 2020 comparably attributable to anthropogenic emission reductions and meteorology. Environ. Res. Lett. 16 (12), 124069. https://doi.org/10.1088/1748-9326/ac3e22.

Yu, S., 2019. Fog geoengineering to abate local ozone pollution at ground level by enhancing air moisture. Environ. Chem. Lett. 17, 565–580. https://doi.org/10.1007/s10311-018-0809-5.

Zhai, S., Jacob, D.J., Wang, X., Shen, L., Li, K., Zhang, Y., Gui, K., Zhao, T., Liao, H., 2019. Fine particulate matter ($PM_{2.5}$) trends in China, 2013–2018: separating contributions from anthropogenic emissions and meteorology. Atmos. Chem. Phys. 19, 11031–11041. https://doi.org/10.5194/acp-19-11031-2019.

Zhai, S., Jacob, D.J., Wang, X., Liu, Z., Wen, T., Shah, V., Li, K., Moch, J.M., Bates, K.H., Song, S., Shen, L., Zhang, Y., Luo, G., Yu, F., Sun, Y., Wang, L., Qi, M., Tao, J., Gui, K., Xu, H., Zhang, Q., Zhao, T., Wang, Y., Lee, H.C., Choi, H., Liao, H., 2021. Control of particulate nitrate air pollution in China. Nat. Geosci. 14, 389–395. https://doi.org/10.1038/s41561-021-00726-z.

Zhang, L., Chen, Y., Zhao, Y., Henze, D.K., Zhu, L., Song, Y., Paulot, F., Liu, X., Pan, Y., Lin, Y., Huang, B., 2018b. Agricultural ammonia emissions in China: reconciling bottom-up and top-down estimates. Atmos. Chem. Phys. 18, 339–355. https://doi.org/10.5194/acp-18-339-2018.

Zhang, Q., Ma, Q., Zhao, B., Liu, X., Wang, Y., Jia, B., Zhang, X., 2018a. Winter haze over North China Plain from 2009 to 2016: influence of emission and meteorology. Environ. Pollut. 242, 1308–1318. https://doi.org/10.1016/j.envpol.2018.08.019.

Zhang, Z., Zeng, Y., Zheng, N., Luo, L., Xiao, Hongwei, Xiao, Huayun, 2020. Fossil fuel-related emissions were the major source of NH_3 pollution in urban cities of northern China in the autumn of 2017. Environ. Pollut. 256, 113428. https://doi.org/10.1016/j.envpol.2019.113428.

Zhang, Q., Zheng, Y., Tong, D., Shao, M., Wang, S., Zhang, Y., Xu, X., Wang, J., He, H., Liu, W., Ding, Y., Lei, Y., Li, J., Wang, Z., Zhang, X., Wang, Y., Cheng, J., Liu, Y., Shi, Q., Yan, L., Geng, G., Hong, C., Li, M., Liu, F., Zheng, B., Cao, J., Ding, A., Gao, J., Fu, Q., Huo, J., Liu, B., Liu, Z., Yang, F., He, K., Hao, J., 2019. Drivers of improved $PM_{2.5}$ air quality in China from 2013 to 2017. Proc. Natl. Acad. Sci. USA 116, 24463–24469. https://doi.org/10.1073/pnas.1907956116.

Zhao, H., Chen, K., Liu, Z., Zhang, Y., Shao, T., Zhang, H., 2021. Coordinated control of $PM_{2.5}$ and O_3 is urgently needed in China after implementation of the "Air pollution prevention and control action plan". Chemosphere 270, 129441. https://doi.org/10.1016/j.chemosphere.2020.129441.

Zheng, H., Kong, S., Chen, N., Yan, Y., Liu, D., Zhu, B., Xu, K., Cao, W., Ding, Q., Lan, B., Zhang, Z., Zheng, M., Fan, Z., Cheng, Y., Zheng, S., Yao, L., Bai, Y., Zhao, T., Qi, S., 2020a. Significant changes in the chemical compositions and sources of $PM_{2.5}$ in Wuhan since the city lockdown as COVID-19. Sci. Total Environ. 739, 140000 https://doi.org/10.1016/j.scitotenv.2020.140000.

Zheng, H., Kong, S., Zheng, M., Yan, Y., Yao, L., Zheng, S., Yan, Q., Wu, J., Cheng, Y., Chen, N., Bai, Y., Zhao, T., Liu, D., Zhao, D., Qi, S., 2020b. A 5.5-year observations of black carbon aerosol at a megacity in Central China: levels, sources, and variation trends. Atmos. Environ. 232, 117581 https://doi.org/10.1016/j.atmosenv.2020.117581.

Zheng, H., Kong, S., He, Y., Song, C., Cheng, Y., Yao, L., Chen, N., Zhu, B., 2023. Enhanced ozone pollution in the summer of 2022 in China: the roles of meteorology and emission variations. Atmos. Environ. 301, 119701 https://doi.org/10.1016/j.atmosenv.2023.119701.

Zheng, B., Tong, D., Li, M., Liu, F., Hong, C., Geng, G., Li, H., Li, X., Peng, L., Qi, J., Yan, L., Zhang, Y., Zhao, H., Zheng, Y., He, K., Zhang, Q., 2018. Trends in China's anthropogenic emissions since 2010 as the consequence of clean air actions. Atmos. Chem. Phys. 18, 14095–14111. https://doi.org/10.5194/acp-18-14095-2018.

Zheng, M., Wang, Y., Bao, J., Yuan, L., Zheng, H., Yan, Y., Liu, D., Xie, M., Kong, S., 2019. Initial cost barrier of ammonia control in Central China. Geophys. Res. Lett. 46, 14175–14184. https://doi.org/10.1029/2019GL084351.

Zheng, B., Zhang, Q., Geng, G., Chen, C., Shi, Q., Cui, M., Lei, Y., He, K., 2021. Changes in China's anthropogenic emissions and air quality during the COVID-19 pandemic in 2020. Earth Syst. Sci. Data 13, 2895–2907. https://doi.org/10.5194/essd-13-2895-2021.

Zhu, X., Ma, Z., Li, Z., Wu, J., Guo, H., Yin, X., Ma, X., Qiao, L., 2020. Impacts of meteorological conditions on nocturnal surface ozone enhancement during the summertime in Beijing. Atmos. Environ. 225, 117368 https://doi.org/10.1016/j.atmosenv.2020.117368.

Zhu, Q., Yu, Y., Gong, H., Wang, Y., Wang, H., Wang, W., Xu, B., Cheng, T., 2023. Spatio-temporal characteristics of $PM_{2.5}$ and O_3 synergic pollutions and influence factors in the Yangtze River Delta. Front. Environ. Sci. 10, 1104013. https://doi.org/10.3389/fenvs.2022.1104013.

Further reading

Liu, X., Niu, J., Wang, Z., Pan, X., Su, F., Yao, D., Zhu, M., Yan, J., Yan, J., Yao, G., 2023b. A comprehensive investigation of $PM_{2.5}$ in the Huaihe River Basin, China: separating the contributions from meteorology and emission reductions. Atmos. Pollut. Res. 14 (1), 101647. https://doi.org/10.1016/j.apr.2023.101647.